LAPPEENRANTA-LAHTI UNIVERSITY OF TECHNOLOGY LUT
School of Engineering Science
Technical Physics degree program

Tatiana Gasiak

FERROELECTRIC PROPERTIES OF LEAD ZIRCONATE-TITANATE (PZT) SINGLE CRYSTALS AND LEAD MAGNESIUM-NIOBATE (PMN) CERAMICS

Examiners: Professor Erkki Lähderanta
D.Sc. Ekaterina Soboleva

Supervisors: Ph.D. Koroleva Ekaterina
Professor Erkki Lähderanta
D.Sc. Ekaterina Soboleva
D.Sc. Pavel Geydt

Abstract

Lappeenranta-Lahti University of Technology

School of Engineering Science

Degree program in Technical Physics

Tatiana Gasiak

Ferroelectric properties of lead zirconate-titanate (PZT) single crystals and lead magnesium-niobate (PMN) ceramics

Master's thesis

2021

Examiners: Professor Erkki Lähderanta

D.Sc. Ekaterina Soboleva

62 pages, 41 figures, 11 tables.

Keywords: ferroelectrics, PZT, PMN, piezoresponse force microscopy, dielectric spectroscopy

The samples of $Pb[Zr_{0.989}Ti_{0.011}]O_3$ (PZT 1.1) single crystal and $0.8Pb[Mg_{1/3}Nb_{2/3}]O_3$ - $0.2PbTiO_3$ (PMN PT20) ceramics were investigated. PMN PT20 ceramics was measured with the dielectric spectroscopy method. Relaxation peak was detected that refers to PMN PT20 phase transition. Both samples were measured with piezoresponse force microscopy (PFM). Polarization experiments were provided. The PZT crystal showed a different piezoelectric response at different areas of the sample surface, which corresponds to its inhomogeneity.

Acknowledgements

I would like to express my gratitude to my supervisors from St. Petersburg Polytechnic University Koroleva Ekaterina Yiurievna, who guided me during whole my scientific work, Prof. Vakhrushev Sergey Borisovich and Vakulenko Alexander Felixovich for the help with AFM measurements. Furthermore, I am graceful to my supervisors from Lappeenranta University of Technology Prof. Erkki Lähderanta and Pavel Geydt for concern. Especial thanks to Soboleva Ekaterina, who helped me during all stages of this work, and without whom it would not be possible.

I am very thankful to School of Engineering Science of Lappeenranta University of Technology and to Physical Engineering High School for the opportunity to study in such appreciable university of Finland.

I would also like to thank my parents and sister for supporting me during studies.

May 2021

Gasiak Tatiana

Table of contents

List of symbols and abbreviations

AC	Alternative current
AFM	Atomic force microscopy
DC	Direct current
FERAM	Ferroelectric random access memory
MPB	Morphotropic phase boundary
PFM	Piezoresponse force microscopy
PMN	Lead magnesium niobate
PMN PT	Lead magnesium niobate - Llead titanate
PZT	Lead zirconate titanate
STM	Scanning tunneling microscope

C	Curie constant
C*	Complex capacity
C_0	Air condenser capacity
F_R	Rhombohedral ferroelectric phase
F_T	Tetragonal ferroelectric phase
I	Current
I*	Complex current
I’	Real part of current
I”	Imaginary part of current
I_0	Amplitude of current
P_s	Saturation polarization
t	Time
T_c	Curie temperature
U	Voltage
U*	Complex voltage
U_0	Amplitude of voltage
Z	Tip-sample distance
Z*	Complex impedance

Z’	Real part of impedance
Z”	Imaginary part of impedance
Zav	Average height/distance between tip and surface
ΔZ	Cantilever deflection
ε*	Complex permittivity
ε	Permittivity
ε’	Real part of permittivity
ε”	Imaginary part of permittivity
θ	Curie-Weiss temperature
φ	Phase shift
ω	Cyclic frequency

1 Introduction

Nowadays, the production of electronic devices is experiencing rapid growth. The constant power increase and miniaturizing require the introduction of new materials with advanced properties for electronic components to follow the expanding requirements. Important types of promising materials are piezo- and ferroelectric materials. They are interesting for their mechanical and electrical properties, which are used in many electronic devices.

The most attractive ferroelectric materials for researchers are complex lead containing oxides lead zirconate titanate (PZT) and lead magnesium niobate (PMN)[1]. PZT materials evince high piezoelectric properties and are easy to produce. That is why they are commonly used in modern devices in various fields, such as actuators, engines, medical and geological devices.

PMN materials are mostly used for research methods, as they appear to be model relaxor class ferroelectrics. Unlike typical ferroelectric materials, which have distinct phase transition point, relaxors show smooth transition in wide range of temperatures and frequencies. From the point of view of practical applications, solid solutions of lead-containing ferroelectric relaxors with lead titanate are expected as the most interesting. They demonstrate record piezoelectric properties near the morphotropic phase boundary (MPB). Recently, it was shown that the relaxor behavior of the PMN lead titanate (PMN PT) solid solution near the MPB is associated with the competition of local interactions: antiferroelectric and ferroelectric, as well as atomic ordering.

However, PZT and PMN materials are widely spread, there is no complete understanding of their electric characteristics. They contain polarization mechanisms depending on microstructural nature of the materials, investigation of structural phases and phase transitions, electric behavior of the materials depending on compounds, electric field and temperature conditions. It was decided to investigate PZT and PMN samples in order to expand knowledge on some of these problems.

For our research we focused on measuring PZT single crystal and PMN PT20 ceramic behavior under electric field. Two different methods of the samples' investigation were used. They are dielectric spectroscopy (used only for PMN PT20 measuring) and piezoresponse force microscopy (PFM). Dielectric spectroscopy provides understanding of

dielectric properties in bulk material for wide range of frequencies and temperatures. PFM allows to investigate response of the sample surface under voltage and temperature conditions.

2 Piezoelectric/Ferroelectric materials

2.1 Piezoelectric and inversed piezoelectric effect

History

Piezoelectric effect was discovered by two brothers – Jacques and Pierre Curie in 1880. They noticed that mechanical force applied to quartz and some other crystals make them electrically polarized. Compression and tension of these crystals produce voltage proportional to the applied force with opposite direction. The ability of creating electricity after tension was found in certain crystals, ceramics and now also known in some biological objects like bones or genetic code molecules, called piezoelectric materials.

Later they proved the opposite assumption: if some voltage is applied to piezoelectric material, it enlarges or shortens accordingly to the polarity of the applied voltage, and its changes are proportional to the value of applied voltage. This effect was called inversed piezoelectric effect.[2]

How it works

The piezoelectric effect can be seen with simple circuit, which contains piezoelectric material placed between metal plates, wires and voltage detector (See Fig. 2.1.1). The piezoelectric material should be compressed or squeezed to generate electricity. After mechanical stress, the material separates charges inside what creates electric potential along it. Metal plates collect charges and put them into the circuit (Fig.2.1.1) where they are detected. In this case, piezoelectric sample behaves like a small battery, unless all piezoelectric materials are non-conductive.

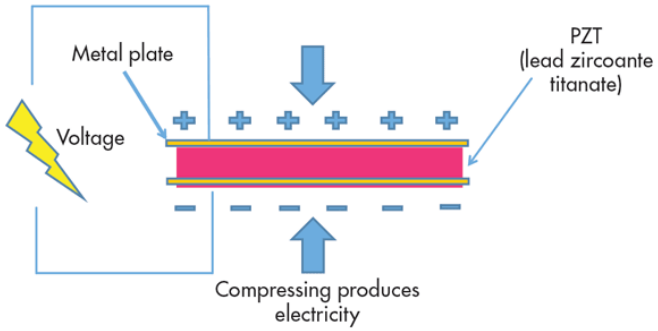

Figure 2.1.1. Detecting piezoelectricity[3].

The inverse piezoeffect can be seen when electrical detector is replaced by generator of electric signal (Fig.2.1.2). The applied alternating voltage make piezoelectric sample mechanically vibrate at the frequency produced by generator. This effect can create sound waves. It is worth to mention that values and amplitudes of mechanical stress and piezoelectricity generated by piezoelectric material are quite small. Therefore, these parameters are usually amplified. The amplifications should be performed carefully avoiding the material destruction.[3]

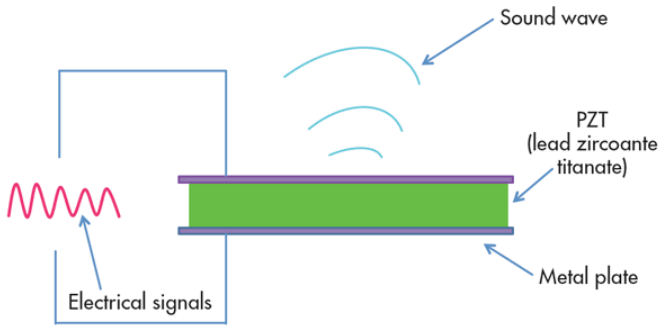

Figure 2.1.2. Inverse piezoelectric effect [3].

Applications

Piezoelectric materials are widely used in everyday life devices. Device production uses two types of piezoelectric materials: crystals and ceramics. Both of these types have the same piezoelectric properties, like piezoelectric strain coefficient, electromechanical coupling and dielectric constant with similar values. Piezoelectric crystals exhibit anisotropic properties, which means they have different piezoresponse values depending on the cut plane relative to the crystal axes. Piezoelectric ceramics are polycrystals representing a compilation of disordered domains, with piezoelectric properties similar in all directions. Therefore, they require larger additional electric field to polarize all their domains. Also, ceramics are easier to manufacture.

Piezoelectric materials are common for electronic device production. They are main components of microphones in cellular phones. Piezoelectric crystals turn sound energy of the voice into electrical signal. This signal is sent to other phone equipped with the same piezoelectric crystal. Now, electrical signal is transferred back into the sound. Same principle is used in sonars. They measure distances to the object by producing and receiving sound. Additionally, piezoelectric materials are used in medical field for ultrasonic devices.

Other applications are force and displacement sensors, mechanical drivers, motors and actuators. Nowadays piezoelectric thin films are coming more and more popular because of their tiny sizes and variation of piezoresponse parameters in a wide range. Their properties' investigation and experiments with composition are among the most attractive research topics [4][5].

2.2 Ferroelectric effect

Main idea

The ferroelectricity was first discovered in Rochelle salt ($KNaC_4H_4O_6 \cdot 4H_2O$) by Valasek in 1921. Ferroelectricity is an effect of spontaneous electric polarization in certain materials. This polarization appears in domains and can be reversed by applied electric field (Fig.2.2.1). Ferroelectricity was called analogously to ferromagnetism, which is shown in tiny magnets aligned to magnetic domains that can be oriented by external magnetic field. That appears in some materials, such as iron. Like polarized domains in ferroelectrics, these magnetic domains could be reoriented with application of external magnetic field [6][2].

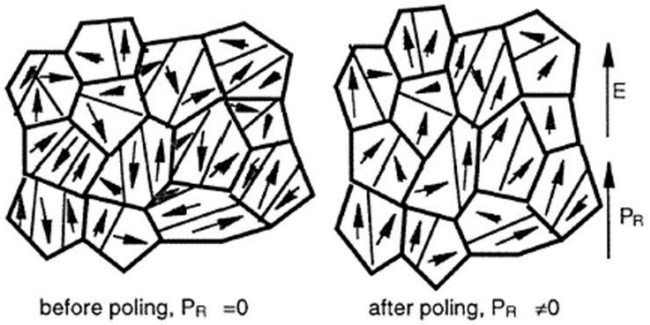

Figure 2.2.1. Ferroelectric domains before and after applying electric field [7] .

Polarization appears when centers of positive and negative charge in crystal structure are separated and dipoles are created out of each elemental crystal cell (Fig.2.2.2 right). The combination of these dipoles unite in domains with positive and negative electric charges on different ends of them. Each domain has random direction of polarization, so in total the material is unpolarized. Moreover, the domain orientation could be controlled by external electric field.

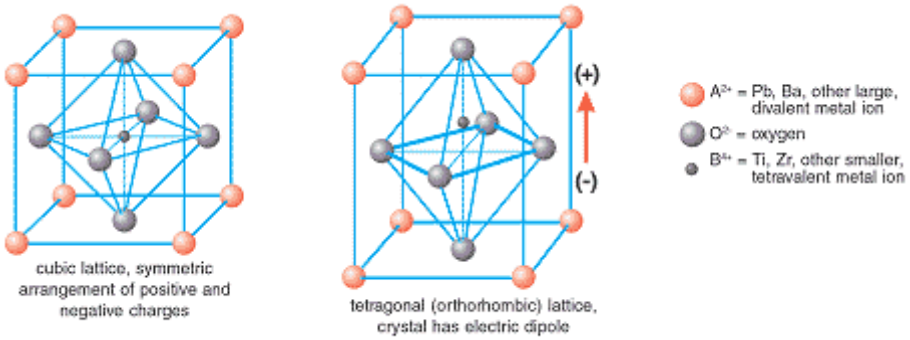

Figure 2.2.2. Crystal structure of PZT-type ferroelectric, above and below Curie point [4].

The presence of a certain crystal structure can explain some specific electrical properties of different materials. According to crystallography, ferroelectric materials are subtype of pyroelectric materials. All of them are piezoelectrics (see table 2.2.1).

Table 2.2.1. Types of materials due to their crystal structure [8].

<table>
<tr><th colspan="5">32 Crystalline classes</th></tr>
<tr><th colspan="4">21 noncentrosymmetric</th><th>11 centrosymmetric</th></tr>
<tr><th colspan="3">20 classes piezoelectric</th><td></td><td rowspan="3">non piezoelectric</td></tr>
<tr><th colspan="2">10 classes pyroelectric</th><td colspan="2" rowspan="2">non pyroelectric</td></tr>
<tr><th>ferroelectric</th><td>non ferroelectric</td></tr>
<tr><td>e.g. : $PbZr/TiO_3$, $BaTiO_3$, $PbTiO_3$</td><td>e.g. : Tourmaline, ZnO, AlN</td><td colspan="2">e.g. : Quartz, Langasite</td></tr>
</table>

Crystal structures are divided into 32 point groups in crystallography. 21 of them are non-centrosymmetric. 20 of these groups are piezoelectrics, i.e., they create electric dipoles when mechanical stress is applied. There are 10 groups among 20 piezoelectric point groups which have polar axis. It provides the material definite polarization with no dependence on type of applied stress (mechanical tension or electric field). These materials are called pyroelectrics, some of them have ferroelectric properties. In fact, there is no structural difference between pyroelectric and ferroelectric materials.

Electric properties

Ferroelectric materials show spontaneous electric polarization after external electric field is applied. They leave some residual polarization after turning off the applied field. Residual polarization appears in non-linear dependencies of polarization through electric field (Fig.2.2.3) [9][10].

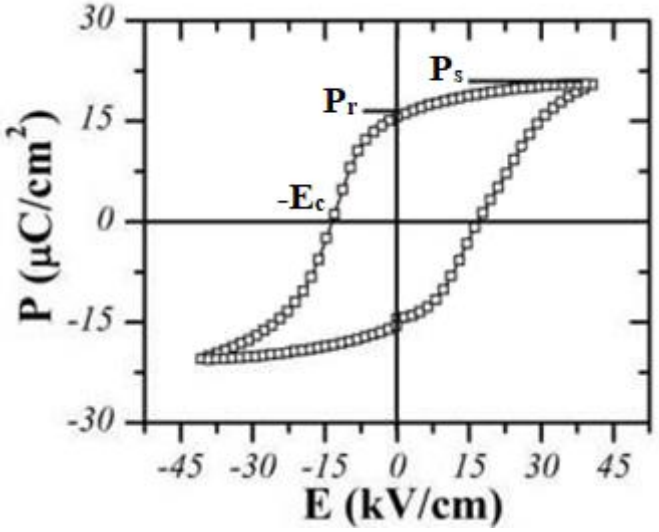

Figure 2.2.3. Polarization versus electric density curve of ferroelectric [8].

Polarization versus the electric field occurs as a hysteresis loop for ferroelectrics. Therefore, polarization of ferroelectric is increasing until some saturation value P_s with increasing of electric field. Polarization decreases slowly when the field gets weaker. Zero electric field causes remnant polarization, P_r, in ferroelectric. The reverse change of field reorientates electric dipoles. Therefore, polarization becomes zero with certain field, called coercive electric field, E_c. If the reversed field continues increasing, polarization will again reach its saturation but in opposite direction. The same behavior is observed when electric field returns to initial direction.

Transitions

Ferroelectric state exists at low temperatures, as at high temperatures there is no spontaneous polarization. The disappearance of ferroelectric properties turns at certain temperature T_c. The crossing of this point leads to change in the material to paraelectric state, called Curie point. The crossing this point leads to change in the material to paraelectric state [2][11].

Moreover, ferroelectrics have high dielectric constant at both low and high temperatures. Permittivity of these materials follows Curie-Weiss law presented by equation (1):

$$\varepsilon' = \frac{C}{(T-\theta)} \tag{1}$$

where *C* is Curie constant and θ is Curie-Weiss temperature. Therefore, relative permittivity curve shows high peak at transition temperature (Fig.2.2.4). Different factors can influence on permittivity values, e.g. the sample porosity, the presence of secondary phases, the level of inhomogeneity, existence / concentration / location / type of defects, grain size, and material conductivity.

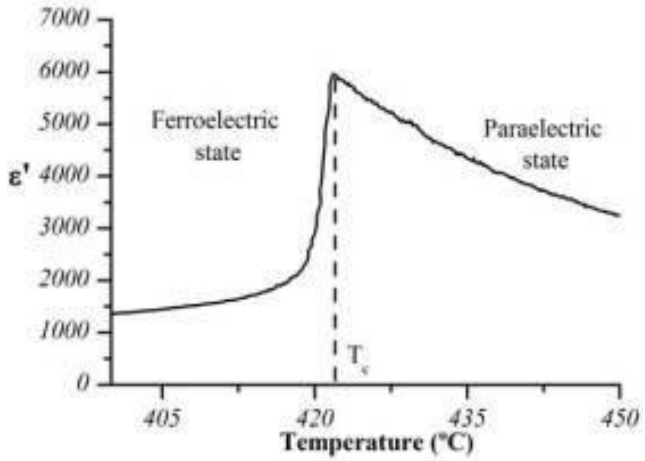

Figure 2.2.4. Phase transition of ferroelectric at Curie temperature [8].

However, the shape of this dependence can also be different (Fig.2.2.5). Sharp peak shows usual phase transition, broadened peak corresponds to diffused phase transition. Additionally, permittivity can depend on frequency of applied field that appears in broad multi-curve. Ferroelectric materials with such behavior are called relaxors [9][8].

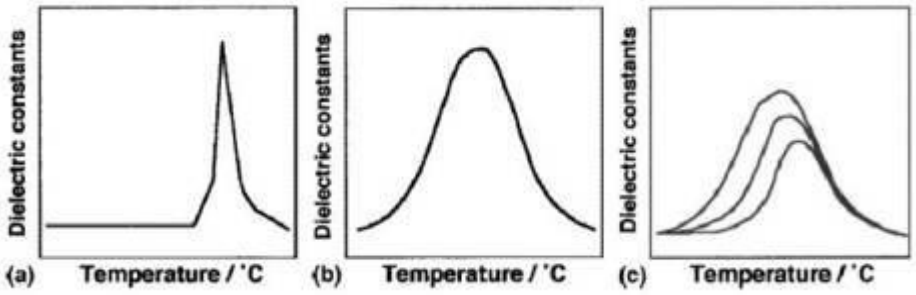

Figure 2.2.5. Permittivity curves for different types of phase transition in ferroelectrics: (a) ”normal” transition, (b) diffused transition, (c) transition in relaxor, measured with different frequencies [12].

Applications

All ferroelectrics are subtypes of piezoelectrics. Therefore, they are used in all the fields where piezoelecrics can be used. Moreover, their electric properties make them more efficient than most of non-ferroelectric piezoelectric materials. Their polarization behavior allows them to be used in tuning capacitors and memory cells, called ferroelectric

random access memory (FERAM). Additionally, producing ferroelectric thin films is very popular for researchers and developers. It means creation of efficient nanoscale devices based on these materials.

2.3 PZT and PMN PT

2.3.1 Lead zirconate titanate (PZT)

PZT is a ferroelectric material with formula $Pb[Zr_xTi_{1-x}]O_3$, where *x* has values from 0 to 1. It was discovered by Sawaguchi et al. at the Tokyo Institute of technology around 1952 [13]. PZT is one of the most widely used materials among ferroelectrics and piezoelectrics unless it referred to be a harmful material. The reasons for its popularity are high dielectric and piezoelectric properties, physical and chemical stability and quite cheap producing. Moreover, the properties could be changed through different zirconium-titanium ratio and adding certain dopants [14].

Electronic device manufacturing commonly uses two types of PZT. Soft PZT ceramics are doped with donors and are used for sensor applications, for example ultrasonic non-destructive testing. Their main characteristics are high density with a fine grain structure, a high Curie point and a noise-free frequency response. Hard PZT ceramics are doped with acceptors and they are used for sonar devices or ultrasonic cleaners, as they require high power characteristics. Their main properties are a high piezoelectric charge constant, higher than soft PZT mechanical quality factor that reduces mechanical loss and enables a lower operating temperature, a low dissipation factor that ensures cooler, more economical operation, high dielectric stability and low mechanical loss under demanding conditions [4].

Structure

Typical PZT has perovskite structure. Its elemental cell contains small tetravalent metal ion surrounded by big divalent ions (Fig.2.3.1). Tetravalent ion is usually titanium or zirconium. Divalent ions are lead ions. The tetravalent metal ions in perovskite are located at the sites of a weakly distorted cubic lattice. Divalent lead ions are located in the centers

of the pseudocubes. Oxygen atoms form almost regular octahedra around titanium/zirconium atoms, which are slightly unfolded and tilted relative to ideal positions.

Figure 2.3.1. Perovskite crystal structure of PZT [15].

The structure of PZT turns into rhombohedral or tetragonal symmetry near morphotropic phase boundary (MPB), under certain composition and temperature. When PZT exists in these phases it has initial dipole moment. PZT shows very high dielectric and piezoelectric response near MPB (Fig.2.3.2). This boundary divides rhombohedral and tetragonal ferroelectric phases, and exists for stoichiometric coefficient x=0.52 i.e. $Pb[Zr_{0.52}Ti_{0.48}]O_3$. The causes of appearance a sharp leap of dielectric and piezoelectric properties is still under discussion.[14]

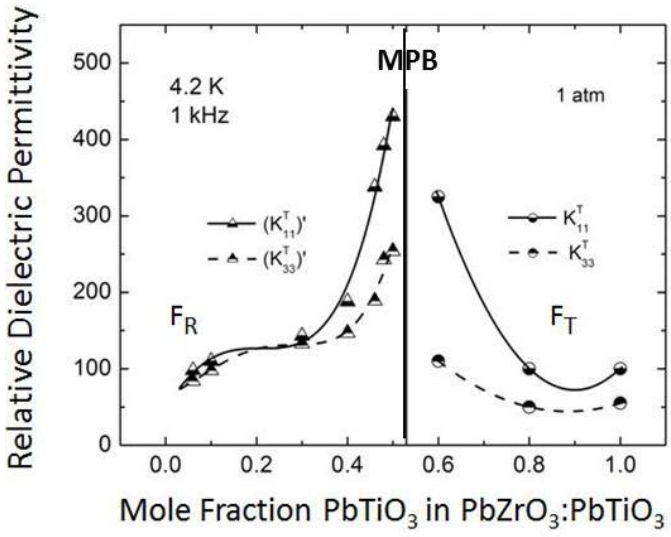

Figure 2.3.2. MPB between rhombohedral (F_R) and tetragonal (F_T) phases in curves of permittivity on mole fraction [14].

2.3.2 Lead magnesium niobate (PMN)

PMN is a ferroelectric relaxor with the formula $PbMg_{1/3}Ni_{2/3}O_3$. It is applied to many technical fields as a part of electronic devices due to its high piezoelectric properties. From this point of view, PMN PT is the material of high interest. The first PMN PT crystals were grown by Park and Shrout using the flux technique [16]. The material shows high piezoelectric coefficient, large piezoelectric strains and very high electromechanical coupling factors. It can be used for high sensitivity sensors like biomedical transducers due to mentioned properties.

Its main characteristic is relaxation dispersion of dielectric permittivity, which is observed in a wide range of frequencies from ~10^{-3} Hz to 10^9 Hz. It is much wider than classical Debye relaxation. PMN has wide and smooth relaxation time spectrum with dependence on the temperature and influences on dielectric permittivity versus frequency. The explanation of such behavior is not fully developed yet. It is believed that dielectric response of PMN is produced by small polarized areas inside non-polarized medium. However, these areas response on applied external electric field is unknown [17].

Structure

PMN also as PMN PT have perovskite type crystal structure. It contains oxygen octahedrons with magnesium or niobium ion inside, that could be replaced by titanium. The structure of PMN PT is shown on figure (2.3.3).

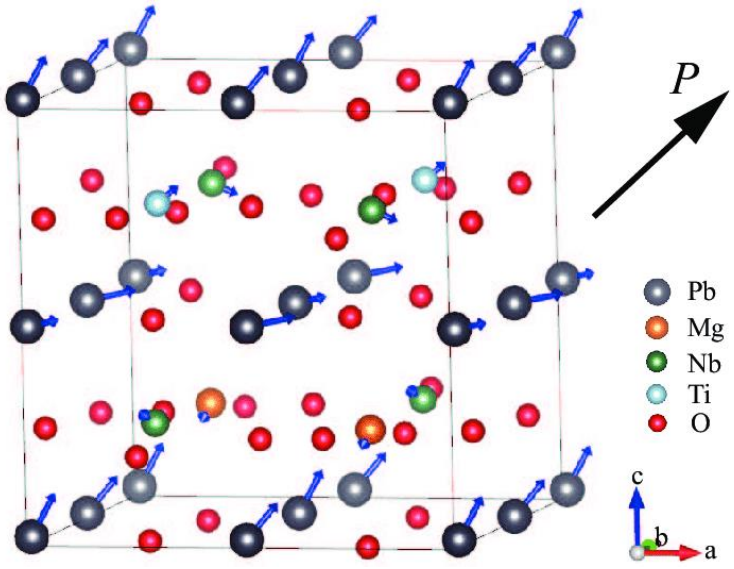

Figure 2.3.3. Crystal structure of PMN PT [18].

The properties of PMN at high temperatures are determined by the coexistence of soft optical phonons that show two-mode behavior and local excitation, associated with hopping of lead ions between several equivalent positions in the oxygen octahedron. Cooling below the so-called Burns temperature, the temperature of appearing randomly polarized ferroelectric nanodomains (~ 630 K for PMN) significantly changes the nature of the lattice dynamics. As a result, a narrow central peak appears in the spectrum. Simultaneously with the dynamic's crossover, there is a change in the form of probability density function for a lead ion. The probability density function forms a spherical layer with decreasing probability of finding undeflected (000) lead. A further decrease in temperature leads to the formation of polar clusters in the regions of the lattice where chemical ordering is observed. As a result, elastic deformation centers appear in the crystal.

The details of the structure of low-temperature PMN and its analogs depend on the composition and cooling conditions. In pure PMN at low temperatures, a glassy phase is formed, while doping of PMN with lead titanate leads to the formation of a regular nanodomain structure, which is confirmed by the study of synchrotron radiation scattering [19][20].

3 Experimental methods

3.1 Dielectric spectroscopy

Dielectric spectroscopy is a technique to study the dielectric properties of materials. It allows to investigate molecular structure, (inter)molecular interactions, kinetics and molecular processes mechanisms in liquids and solid bodies. This knowledge provides deeper understanding of different materials. Dielectric spectroscopy is used in many fields such as electrical and electrochemical devices developing, semiconductor technologies, chemical analysis and medicine producing.

Dielectric spectroscopy is based on measuring electric response of the sample to which alternating current (AC) is applied. These measurements are described as frequency dependences of electric properties. The most important of them are permittivity and electric conductivity. The real and imaginary parts of permittivity are shown in Fig. 3.1.1.

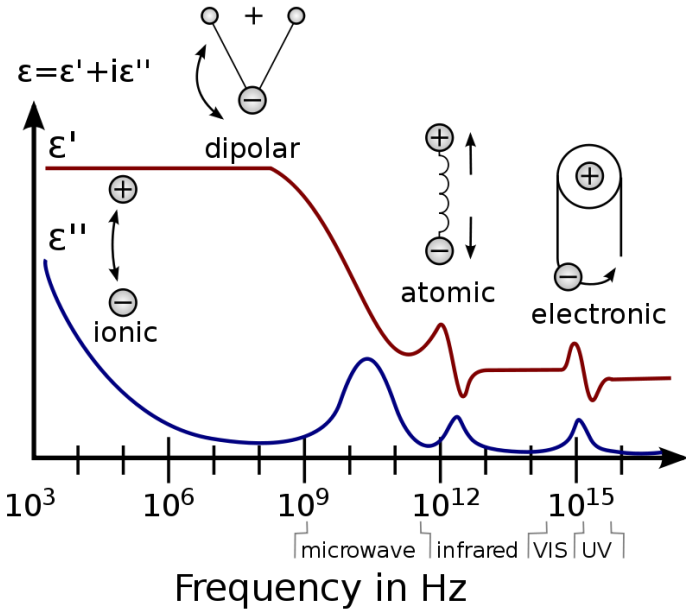

Figure 3.1.1. Frequency dependencies of permittivity and interactions connected with them. Red line corresponds to real part of permittivity, blue line corresponds to imaginary part of permittivity [21].

An assumption that any material consists of dipoles of different sizes was made to describe the work principle of the method. When external electric field is applied, these dipoles tries to orient along its direction. The change of the dipole direction needs some time, called relaxation time. It depends on dipole's dimensions. All the dipoles of the sample create own polarization, which causes the response. The application of alternating

electric field to a material causes the dipole rotation. If frequency of alternating field is high, dipoles do not have enough time to complete their rotation. Therefore, the response gets weaker and energy losses appear. This process can be detected with current and voltage measurements during applying alternating current in a set of different frequencies.

The development of experimental methods to measure dielectric properties created possibility to expand the list of research objects, frequency range and temperature range. Dielectric spectroscopy is sensitive to relaxation processes in an extremely wide range of characteristic times (10^{5} - 10^{-12} s, shown in Fig.3.1.2) [22].

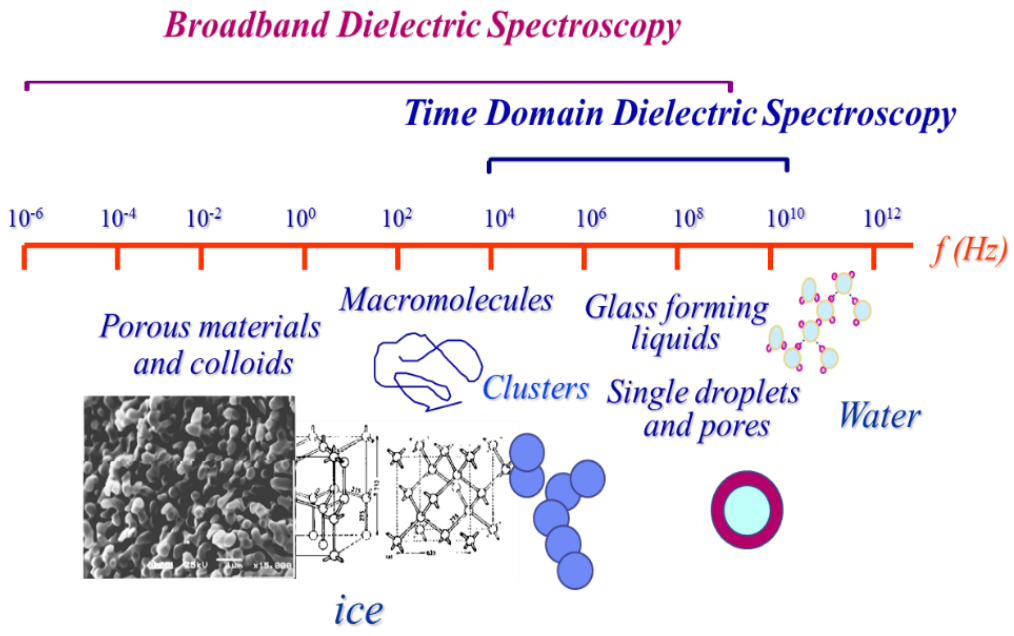

Figure 3.1.2. Frequency range and objects that could be investigated by dielectric spectroscopy [22].

Measuring process

The Figure 3.1.3 shows the principal circuit of measuring electric properties of dielectric materials. The sample is placed between two parallel electrodes that creates a flat capacitor.

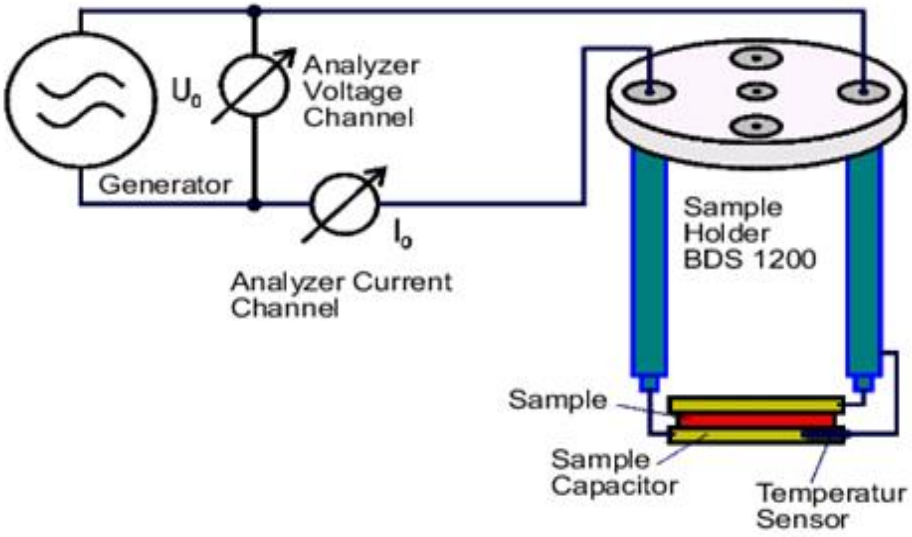

Figure 3.1.3. Principal scheme of the dielectric spectrometer [23].

A voltage with amplitude U_0 and frequency ω/2π is applied to a sample. U_0 causes current I_0, which goes through the sample with the same frequency as the voltage. There is difference in the phases of current and voltage, which is called phase shift φ. Both current to voltage ratio and phase shift depend on dielectric properties of the sample and its dimensions. The voltage and current definitions are given by formulas (2) and (3). The complex values were used to simplify calculations.

$$U(t) = U_0 cos(\omega t) = Re(U^* e^{i\omega t}) \quad (2)$$

$$I(t) = I_0 \cos(\omega t + \varphi) = Re(I^* e^{i\omega t}) \quad (3)$$

where $U^*=U_0$ and $I^* = I' + iI"$, where I' and I'' mean amplitude of real and imaginary part of the current respectively.

I_0 means amplitude of current, expressed with formula (4):

$$I_0 = \sqrt{I'^2 + I"^2} \quad (4)$$

Therefore, the phase shift is calculated by the formula (5):

$$\tan \varphi = \frac{I''}{I'}. \quad (5)$$

Impedance of a material with linear electromagnetic response $Z^* = Z' + iZ'' = \frac{U^*}{I^*}$ is related to its dielectric response function with formula (6):

$$\varepsilon^*(\omega) = \varepsilon' - i\varepsilon'' = \frac{-i}{\omega Z^*(\omega)}\frac{1}{C_0} = \frac{C^*}{C_0} \quad (6)$$

where C_0 is the capacity of an empty cell.

Complex conductivity is related with dielectric response with formula (7):

$$\sigma^* = \sigma' - i\sigma'' = i2\pi f \varepsilon_0(\varepsilon^* - 1)\,. \quad (7)$$

The response of an ideal set of dipoles that do not interact with each other is described by the Debye function (8):

$$\varepsilon(\omega) = \varepsilon_\infty + \frac{\varepsilon_S - \varepsilon_\infty}{1 + i\omega\tau} \quad (8)$$

Here ε_S is static permittivity (at low frequencies), ε_∞ is permittivity at high frequencies, τ is relaxation time of Debye process.

Complex permittivity consists of real and imaginary parts, calculated by formulas (9) and (10):

$$\varepsilon'(\omega) = \varepsilon_\infty + \frac{\varepsilon_s - \varepsilon_\infty}{1 + \omega^2\tau^2} \quad (9)$$

$$\varepsilon''(\omega) = \frac{(\varepsilon_s - \varepsilon_\infty)\omega\tau}{1 + \omega^2\tau^2} \quad (10)$$

The loss peak has symmetric shape shown in the figure 3.1.4. The characteristic width at a half-height of imaginary part of permittivity equals to 1.144 decades.

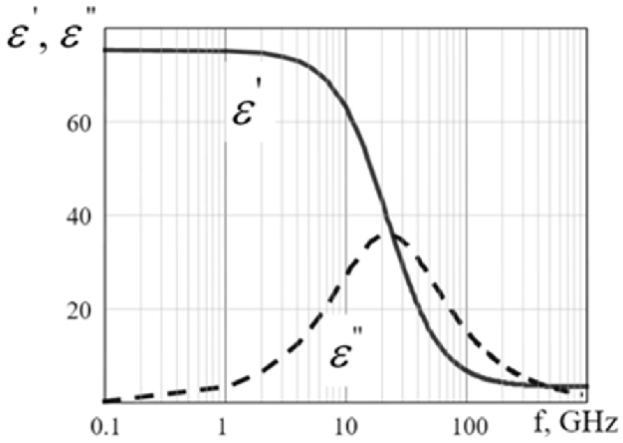

Figure 3.1.4. Debye model of frequency dependencies of the real and imaginary part of permittivity in dielectrics [24].

The plot of the imaginary component of dielectric response against real component is called Cole-Cole diagram. It has a half-of-circle shape with diameter of $\varepsilon_0 - \varepsilon_\infty$ on real axis (Fig.3.1.5).

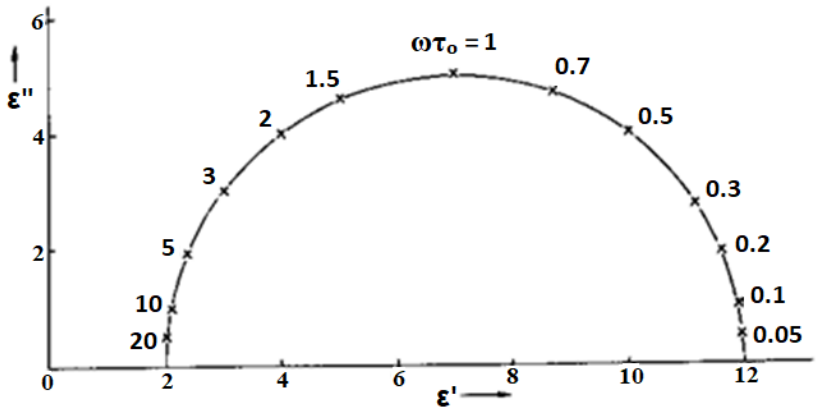

Figure 3.1.5. Cole-Cole diagram for Debye model material with single relaxation time, were ω is measuring frequency and τ_o is relaxation time, the numbers on the curve show their multiplication [25].

Our equipment

In our work, measurements of the electrical properties of the samples were carried on a Novocontrol BDS80 ultrawideband dielectric spectrometer with a Novotherm-HT (RT-1000C) high-temperature furnace (manufacturer Novocontrol Technologies GmbH & Co. KG, Germany). $\omega\tau_o = 1\varepsilon'$

Spectrometer parameters:

1) Frequency range: 3 μHz..20 MHz;

2) Impedance range: 0.01..10^{14} Ohm;

3) Electric capacity range: 1fF..1F;

4) Tangent of the loss angle: 10^{-5}..10^{4};

5) Signal amplitude range: 100 μV..3 V;

6) Measuring response range: -40 V..40 V;

7) Temperature range: -160..400 °C

In our experiment, the samples were investigated with 0.1 Hz – 3 M Hz range of frequencies and 150 – 500 K range of temperatures.

3.2 Piezoresponse Force Microscopy (PFM)

Atomic force microscopy (AFM) is one of the techniques of scanning probe microscopy that investigates sample surface by “feeling” it with a small tip. The first AFM was developed in 1986 by Gerd Binnig, Kalvin Quate, Christoph Gerber [26]. That was a modification of previously invented scanning tunneling microscope. Nowadays the resolution of this method can reach the dimensions of a single atom as it is based on interactions between atoms of surface and tip.

Main principle

AFM consists of probe with cantilever and tip, piezoscanner, optical detecting system, including laser and photodetector (Fig.3.2.1). The working principle is based on detecting of the force interaction between studied surface and the probe. A sharp nanoscale tip (tip radius ~10 nm) is attached to the end of elastic cantilever that is used as a probe. The force acting on the tip from the sample surface bends the cantilever. The appearance of elevations or depressions under the tip leads to a change in the force acting on the probe, and hence to a change in the magnitude of the cantilever bending. This changing is registered by deflection of laser beam on the four-sectioned photodetector. The signal makes a feedback loop that controls the height of the probe above the surface. Detector usually can define about 10^{-2}Å provides deflection of the cantilever. Measuring the deflection in every point of scanning surface provides the image of the surface relief [27].

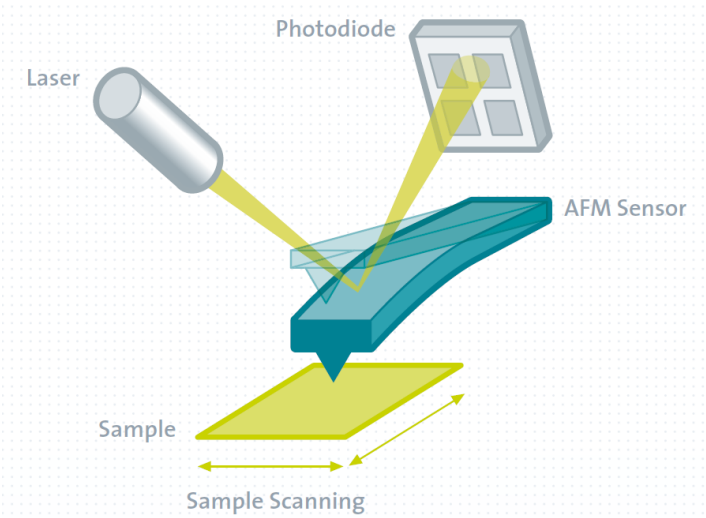

Figure 3.2.1. Scheme of atomic force microscope [28].

The forces acting between the probe and the sample are primarily short-range Van der Waals forces. These forces include components of different signs and provide attraction at large distances, and repulsion at small ones. The energy of the Van der Waals interaction between two atoms located at a distance *r* from each other is approximated by a power function - the Lennard-Jones potential, expressed with the formula (11):

$$U_{LJ}(r) = U_0 \left[-2 \left(\frac{r_0}{r} \right)^6 + \left(\frac{r_0}{r} \right)^{12} \right]. \quad (11)$$

The interatomic force on the distance between the tip and the sample dependence is shown in Fig. 3.2.2. The right side of the curve characterizes the situation when the tip and the surface are separated by a large distance. As they gradually approach each other, at first they will be only weakly attracted, and then more and more attracted to each other. The force of attraction will increase until the atoms come close enough that their electron clouds begin to repel electrostatically. The further decrease in the interatomic distance causes electrostatic repulsion exponentially and weakens the force of attraction. These forces are balanced at a distance between atoms of the order of two Å, which is approximately the length of a chemical bond. When the total interatomic force becomes positive (repulsive), it means that the atoms have come into contact.

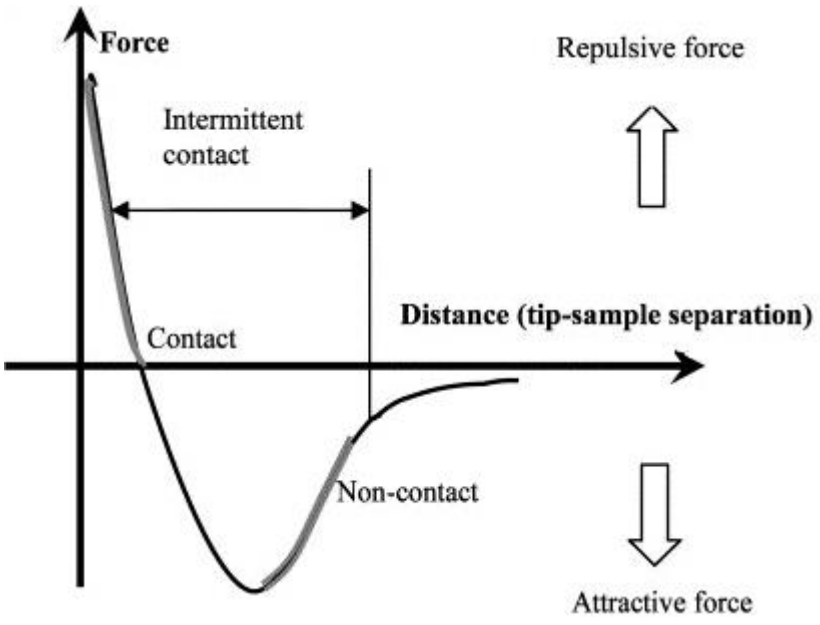

Figure 3.2.2. Intermolecular force on tip-sample distance [29].

In Fig. 3.2.2, zero tip-sample separation corresponds to the zero distance between the atomic nuclei on the sample surface and the cantilever closest to the atom surface. Therefore, the force zero is located at a finite distance corresponding to the boundary of the electron shells of these atoms (when the shells overlap, repulsion occurs). If the position of outer shell of the atom is taken as zero position, then the force will be equal to zero at the zero point of the distance.

Modes

There are three operation modes of the AFM, depending on the distance between probe and surface. They are:

- Contact mode
- Semi-contact mode or tapping mode
- Non-contact mode or contactless mode

Non-contact and tapping modes have common features. In these techniques, the oscillations of the cantilever are excited by an external piezoelectric element (actuator) at the resonant frequency. The control parameter of the feedback loop is the cantilever oscillation amplitude. Therefore, tip-surface interaction changes the amplitude and phase of cantilever oscillation, which is registered and turned into surface image.

In tapping mode with a sufficiently large amplitude, the cantilever breaks the established bond with the sample at each period, thus eliminating the influence of frictional forces and capillary sticking. As the probe approaches the surface, an additional force from the sample begins to interact with the probe. Van der Waals interaction appears in the region of distances between the probe and the sample, where the force of attraction affects.

In non-contact mode the tip oscillates near the surface without touching. The oscillating amplitude is much smaller than in tapping mode. When the distance between tip and surface becomes small enough, the Van der Waals force occurs. Therefore, the force affects on amplitude and phase of the cantilever so these deflections transform into image. Non-contact mode can be performed in 2 ways: constant height or constant forces.

Contact mode

We were mostly interested in contact mode, as it is used for piezoresponse properties investigation. Contact method supposes the direct contact of the tip with the surface, while the elastic force of the cantilever balances the forces of attraction and repulsion acting from the surface of the sample. When AFM operates in such mode, cantilevers with low stiffness coefficients are used, which allows avoiding harmful impact on the sample.

In the contact AFM mode, the measurements could be provided in two ways. One is characterized with constant interaction force of the probe with the surface (force of attraction or repulsion). During scanning in constant force mode, the feedback loop maintains the same cantilever bend value, and therefore the force of pressing the probe on the sample is similar. In this case, the control voltage in the feedback loop applied to the Z-electrode of the scanner will change with changing the height of the sample surface relief.

The second way uses a constant distance between the probe and the sample surface (Z = const). It is commonly used when smooth surfaces are investigated. In this case, the probe moves with a certain average height Z_{av} above the sample, and at each point, the cantilever bend ΔZ is recorded, which is proportional to the force acting on the probe from the surface. The AFM image in this case shows a spatial image of the force of tip-surface interaction.

The advantage of contact AFM method in comparison to optical and electron microscopy methods is its high sensitivity, high resolution of the surface imaging. The disadvantage of this mode is the direct mechanical interaction of the probe with the surface. This often leads to destruction of probes and damage of the sample surface during scanning.

Piezoresponse Force Microscopy (PFM)

PFM is based on the contact force mode of AFM. This method allows investigation of ferroelectric properties of the samples. The scheme of PFM is presented in Fig. 3.2.3.

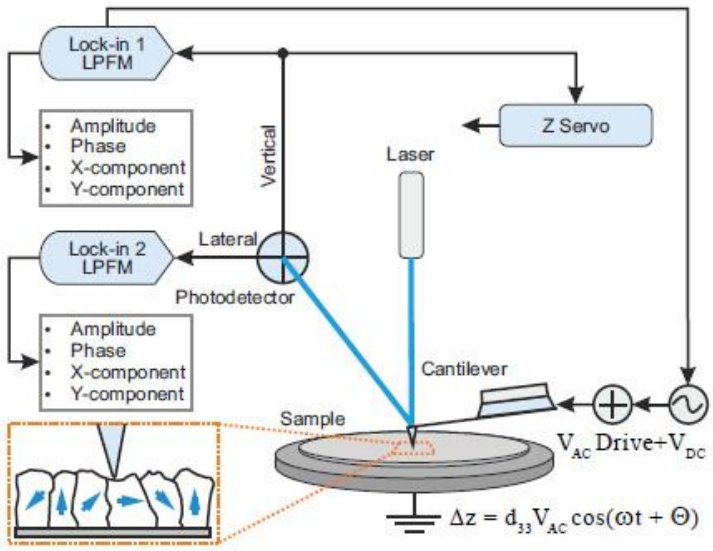

Figure 3.2.3. Principal scheme of piezoresponse force microscope [30].

The main principle of PFM is based on reverse piezoelectric effect. Conductive tip moves along the surface and applies electric field to it. Mechanical defects appear at the point of surface where the tip locates under applied electric field. These defects could be detected by the probe, so the response is collected and converted to piezoresponse images. Using this technique, ferroelectric domains could be measured. Each domain is polarized in its own direction, so additional electrostatic force between tip and sample is created under electric field of the tip. Different domains have different polarization direction that leads to different electrostatic force direction and different piezoelectric response, so the domains are visible on piezoresponse channels (Fig.3.2.4).

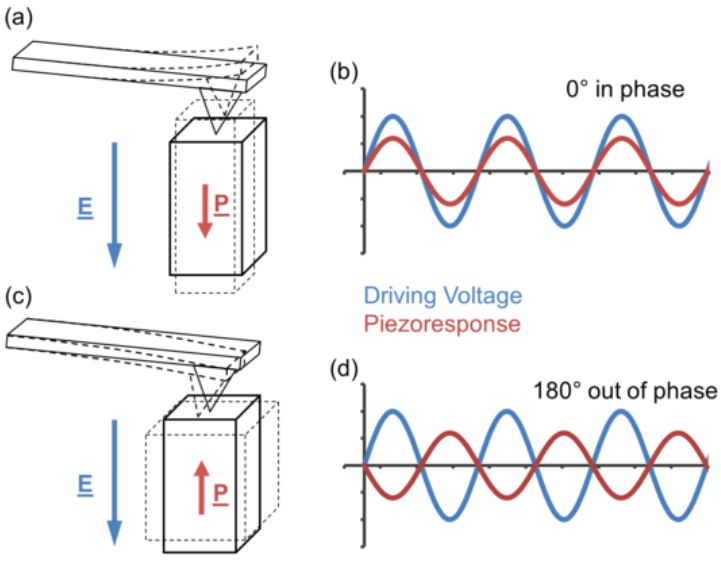

Figure 3.2.4. Interaction of the probe with polarized part of the sample (a), (c) and voltage characteristics of applied electric field and piezoresponse (b), (d) [31].

During the PFM measurements, alternating current is applied to the tip. This makes the sample vibrating with the amplitude ~1 nm. Electrode under the sample is grounded. Piezoelectric and ferroelectric samples can locally extend or retract with dependence on direction of external field. The domains with perpendicular to the surface (out-of-plane) polarization have vertical response after tip voltage. If the sample domain is polarized in the same direction as applied electric field, it enlarges in this direction. Its piezoresponse is synchronized with tip voltage (Fig.3.2.4 (b)). For opposite domain polarization, it retracts and half-period phase shift appears (Fig.3.2.4 (d)). If domain has polarization, parallel to the sample surface (in-plane), the interaction with tip results in lateral movement of the tip.

During measurements, small AC is used. It is needed for non-destructive domain scanning. Domains have their own switching electric field that turns their polarization to the direction of applied electric field. Therefore, if tip bias is over it, the domains will change their polarization. Domains do not switch with fewer AC voltage and their phase contrast shown on piezoresponse images defines polarization of domains. If the sample has only vertically polarized domains, they have ~180° difference for out-of-plane phase channel, not depending on position of the sample surface.

There is a possible case where domains have complex orientation, containing both in-plane and out-of-plane components of polarization. The definition of these domains is provided by vertical and lateral piezoresponse channels. Moreover, if a DC voltage is applied between the probe and the sample in addition to the AC voltage, then both electromechanical responses (in-plane and out-of-plane) of the sample are also a function of the DC voltage.[32]

The electrostatic components contributed to the PFM signal decrease with increasing frequency of the external AC voltage. Non-local components are removed especially fast. In addition, the image obtained at a higher frequency is determined by the stiffness of the cantilever, which improves the contrast between the probe and the sample surface. Therefore, higher frequency PFM images are largely free of electrostatic effects and provide a higher signal-to-noise ratio. The optimal vertical PFM signal can be obtained at frequencies in the MHz range. The lateral PFM signal is usually optimal at a frequency of 10 to 100 kHz depending on the chosen AFM probe and sample. However, a further

increase in the frequency of the external AC voltage affects the upper limit of the frequency range of the photodetector and lock-in amplifier. The signal is not transmitted at extremely high frequencies due to the excessive stiffness of the cantilever.

The piezoresponse image depends on the topographic features of the surface. A large piezoelectric response occurs at the resonant frequency. This frequency depends on “probe-sample” contact stiffness, which is influenced by the area of tip-surface contact. The contact area is determined by surface characteristics. If the tip is located in a convex part of the surface, the “probe-sample” contact stiffness is larger than the tip was located on the flat part. The bigger contact stiffness leads to the higher contact resonant frequency. As the measuring frequency is fixed and corresponds to resonance for flat tip-surface contact, the changes of resonant frequency appear in decreased piezoresponse signal. The main applications of PFM include the local characterization of the electromechanical properties of materials, containing detailed domain mapping and studying domain switching dynamics. PFM is used in testing of micro- and nanoelectromechanical devices (e.g. piezoelectric actuators, transmitters, and micro-electromechanical systems), electro-optical devices, and non-volatile memory (e.g. FERAM), by addressing their reliability, e.g. electromechanical fingerprint, fatigue and dielectric breakdown. PFM allows the investigation of the relationship between local and global polarity and other properties of materials based on new polymers and bioengineered materials by detailed description of the nanometric structure and electrical characteristics of such materials, etc. [33]

Our equipment

In this work, measurements of the ferroelectric properties of the samples were carried with PFM method on a MultiMode 8-HR atomic force microscope (manufacturer Bruker Corporation, USA).

4 Measurements

4.1 Samples

There are different methods of creating PZT single-crystals and PMN ceramics. This work considers two of them.

PZT single crystal

The PZT has composition $Pb(Zr_{0.525}Ti_{0.475})O_3$, which is in the MPB region. The PZT powder is prepared using the reagents $PbCO_3$, TiO_2, and ZrO_2, with a high purity grade (>99%). The powders are mixed for 3 h in a planetary ball milling, in teflon jars, with alcohol medium and zirconia balls. The slurry is dried in an oven at 100ºC for 24 h, calcined at 900ºC for 2 h and grinded in an agate mortar. The flux PbO-KF-$PbCl_2$, in the molar ratio of (2:1:2), is then added. It was prepared using PbO, KF, $PbCl_2$ and B_2O_3, with a high purity grade, >99%. The powders are mixed for 3 h in a planetary ball milling, in teflon jars, with alcohol medium and zirconia balls. The slurry is dried in an oven at 100ºC for 24 h. The materials, PZT and the flux, are put in a platinum crucible of 50 cm^3. The crucible is placed inside a vertical electric furnace. The heat treatment followed the planned conditions, table 4.1.1 shows an example of the heat treatment condition. The flux is then removed by dissolving it in warm diluted nitric acid, 35% in water, and filtered it.[34]

Table 4.1.1. Conditions used for the crystals grown and the corresponding weight losses and compositional results in terms of x in $Pb(Zr_xTi_{1-x})O_3$ [34].

Conditions	Temperature (C°)	Holding time (h)	Cooling rate (°C/h)	Flux percent (wt%)	Weight loss (wt%)	Composition x
C1	1200	5	10	40	22	0.43
C2	1150	5	10	40	23	0.50
C3	1150	5	10	60	28	-
C4	1150	10	10	60	32	0.49; 0.55

PMN PT ceramic

The 0.69PMN-0.31PT ceramics is prepared by the conventional ceramic processing via the columbite precursor method. Analytical-purity oxides, PbO, MgO, Nb_2O_5 and TiO_2 are used as raw materials. In order to maintain chemical stoichiometry, all the raw oxides are fully dried before weighing. In this method, MgO and Nb_2O_5 were reacted at 950°C for 2 h to form the columbite precursor $MgNb_2O_6$ at the initial step. Then stoichiometric Pb_3O_4

and TiO_2 are added into the $MgNb_2O_6$ precursor according to the chemical composition and calcined at 800°C for 2 h to form perovskite 0.69PMN-0.31PT. The calcined powder is cold dry-pressed uniaxially into pellets with the addition of 1.5 wt% polyvinyl alcohol binder and then sintered at 1220°C for 2 h. During the sintering process, the samples are buried under an equiweight mixture of raw oxides with the same composition in a covered crucible to minimize the evaporation of lead.[35][36]

The investigated PZT and PMN PT20 samples were prepared with confidential technique. Unfortunately, it is not yet allowed to provide the information.

PZT single crystal has parallelepiped shape with 2x1.5x1 mm dimensions. PMN PT20 ceramic sample had cylinder shape with 18 mm diameter and 0.8 mm thickness. For dielectric spectroscopy measurements gold electrodes were sputtered on two sides of PMN sample to make good electric contact with spectrometer electrodes. For PFM measurements the PZT single crystal sample was attached by silver conductive paste to conductive disk and the PMN sample was cut to form segment with 8 mm chord length. The part of electrode on one side of PMN was removed, the other side was attached by silver conductive paste to conductive disk.

4.2 Dielectric spectroscopy measurements

Dielectric spectroscopy measurements were performed on ceramic PMN PT20 sample. Temperature and frequency dependencies of real and imaginary part were measured. PZT single crystal was not studied by means of dielectric spectroscopy due to very small sizes.

Firstly, the behavior of the PMN PT20 sample was investigated during heating and cooling using several frequencies without applying additional electric field. Both cooling and heating curves at one plot for 1 Hz measurements are presented in figure 4.2.1.

It is seen that cooling and heating curves repeat each other at low and high temperatures, for real part of permittivity this behavior manifests itself to a greater extent. The differences appear for temperatures from 280 K to 360 K, where permittivity peak is located. This peak corresponds to phase transition of the relaxor.

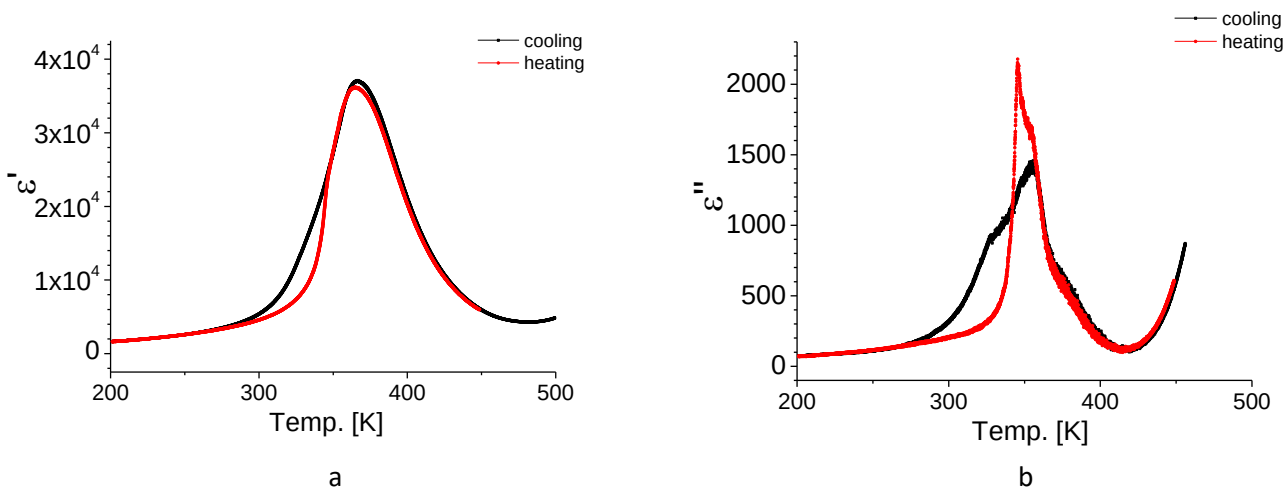

Figure 4.2.1. Temperature dependencies of permittivity with 1 Hz frequency: real part (a) and imaginary part (b), for both cooling and heating without additional electric field for PMN PT20 ceramic sample.

The measurements for different frequencies in a range from 1 Hz to 300 kHz are shown separately in figure 4.2.2. The frequency dependencies for several temperatures are shown in figure 4.2.3.

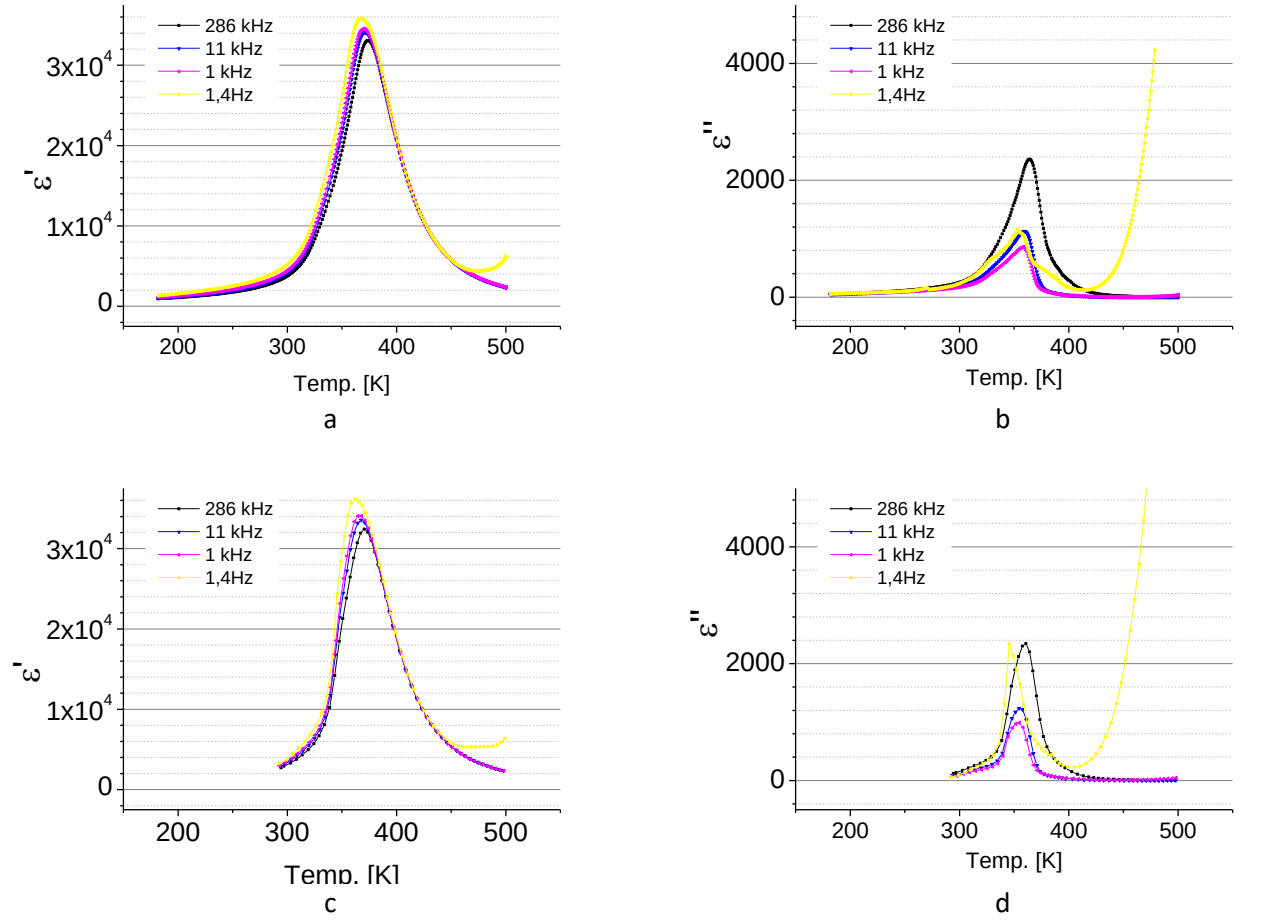

Figure 4.2.2. Temperature dependencies of permittivity: real part (a),(c) and imaginary part (b),(d) at field cooling (a),(b) and zero field heating (c),(d) for PMN PT20 ceramic sample.

Measurement showed similar behavior for several frequencies. The permittivity curve peak occurs at the same range of 360 – 370 K and has similar high of real part of permittivity at 3.3 – 3.6 × 10^4 for all measured frequencies. It is seen that with lower frequency the peak of permittivity real part moves to lower temperature and has more intensity. The movement is the same for imaginary part of permittivity, characterizing dielectric losses of the sample. However, the intensity of imaginary part of permittivity decreases with frequency decreasing until 1 kHz. The intensity of the response rises again for frequency lower than 1 kHz. Moreover, it rapidly increases after 400 K with temperature rising.

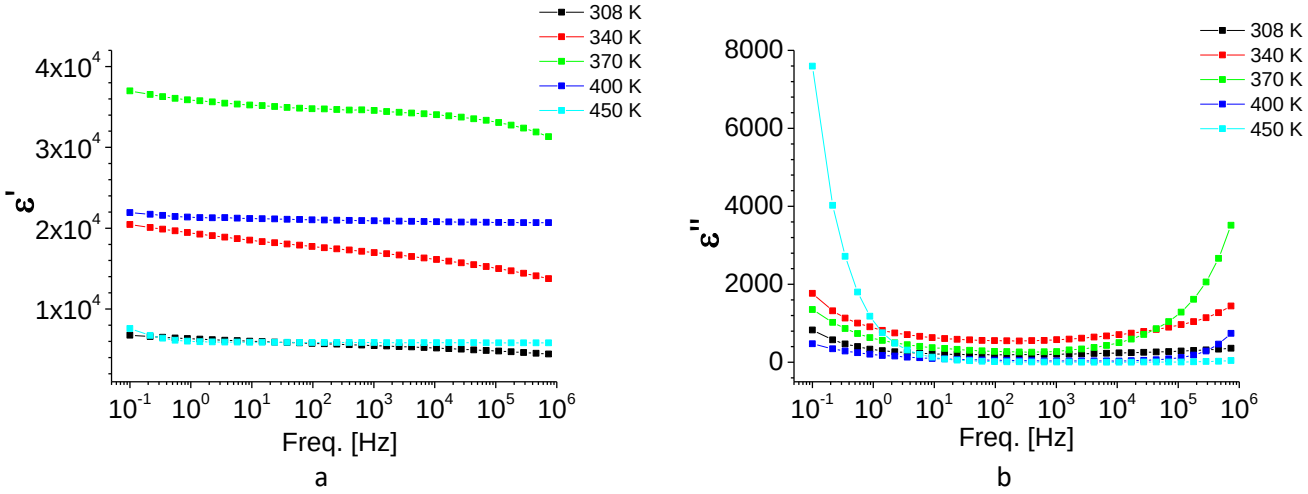

Figure 4.2.3. Frequency dependencies of permittivity: real part (a) and imaginary part (b), for room temperature, 340 K, 370 K, 400 K and 450 K for PMN PT20 ceramic sample.

Frequency dependencies show quite stable dielectric response of the sample in a wide range of frequencies (from 1 Hz to 100 kHz) at all measured temperatures for imaginary part of dielectric response. The real part of dielectric response shows steady frequency dependencies for temperatures higher than 370 K. It is seen that permittivity increases with temperature increasing until 370 K for real part of permittivity and until 340 K for imaginary part, then it starts to decrease. These results correlate with temperature dependencies shown in figures 4.2.1 and 4.2.2, because there is seen rising of dielectric response with temperature increasing until ~370 K for real part of permittivity and until ~350 K for imaginary part of permittivity with a subsequent decrease of dielectric response.

Secondly, measurements were provided with additional bias electric field. The results are presented in figures 4.2.4 and 4.2.5. The sample was heated until 500 K, then bias was applied to electrodes, between which the sample was located. The voltage was

constant (1 kV) while the sample was cooling. After 180 K the electric field was turned off and the sample was heated again. The measurements were done during field cooling and zero field heating.

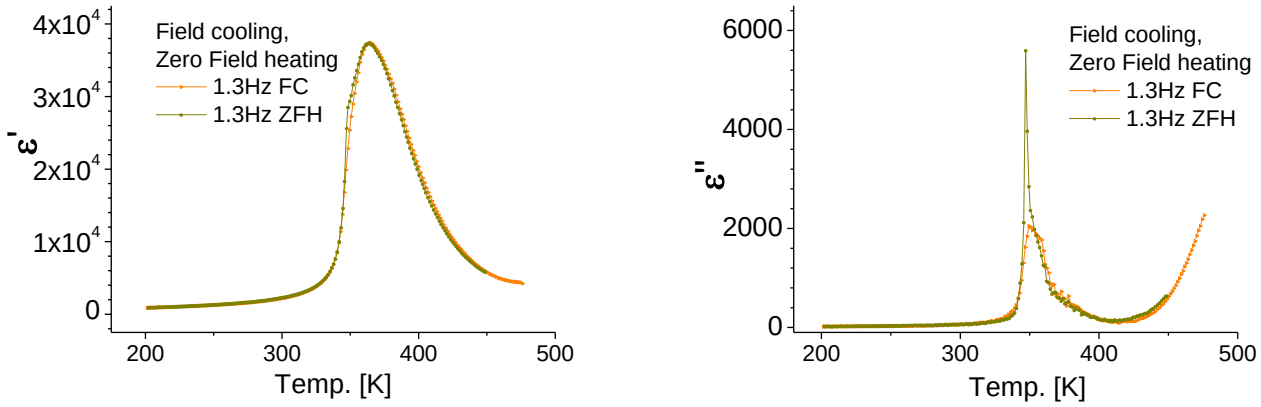

Figure 4.2.4. Temperature dependencies of permittivity: real part (a) and imaginary part (b), for both field cooling and zero field heating for PMN PT20 ceramic sample.

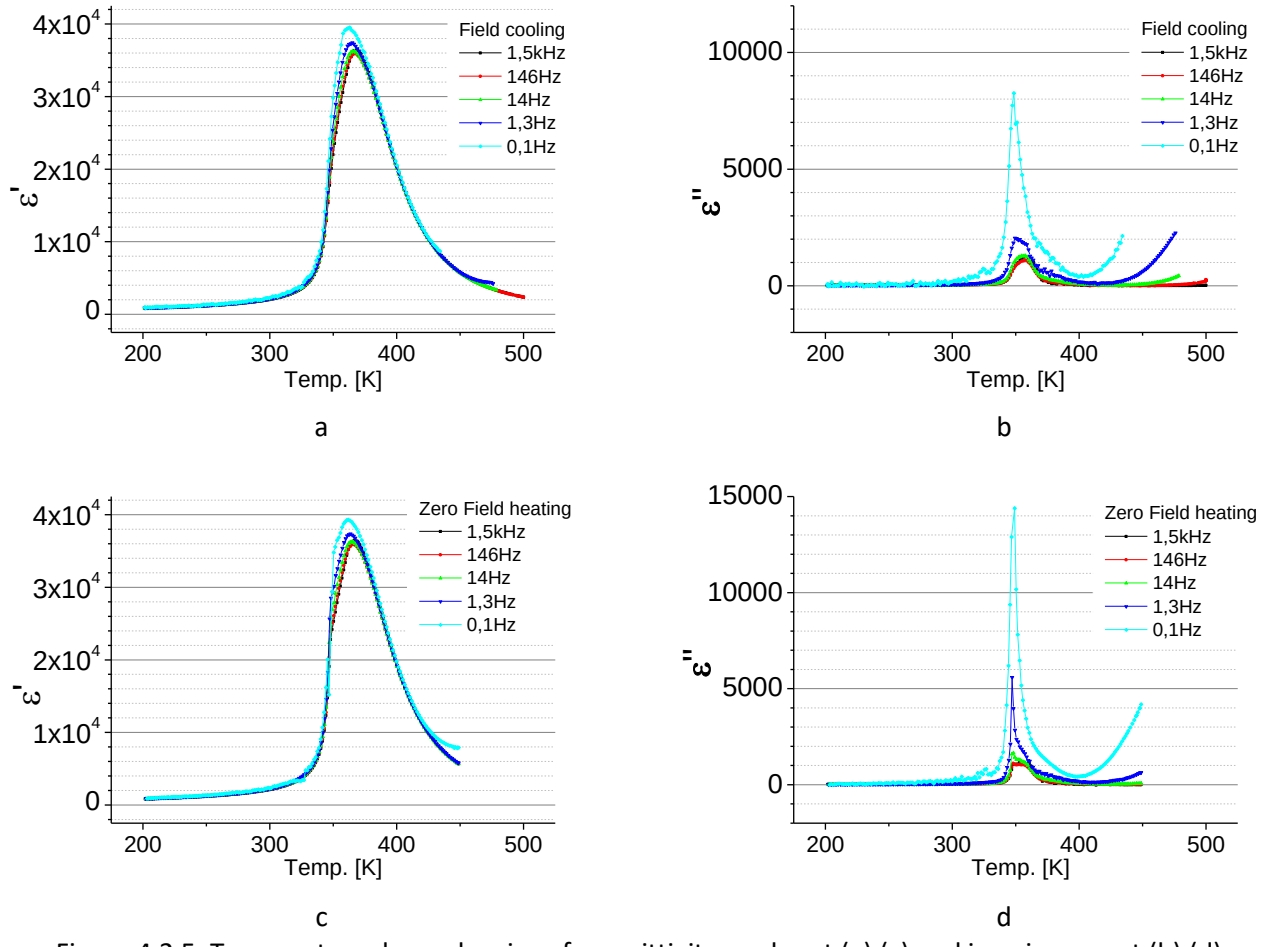

Figure 4.2.5. Temperature dependencies of permittivity: real part (a),(c) and imaginary part (b),(d) at field cooling (a),(b) and zero field heating (c),(d) for PMN PT20 ceramic sample.

The dependencies shown in figures 4.2.4 and 4.2.5 demonstrate similar behavior as for previous experiment (Fig. 4.2.1 and 4.2.2). Both real and imaginary part of permittivity increase in exponential way and then decrease with rising temperature. For real part of dielectric response the peak appears at 365 – 370 K with frequency increase, the amplitude of the peak is $3.4 – 3.7 \times 10^4$. For imaginary part of permittivity the peak occurs at 350 – 360 K with frequency increase, the intensity of peak is higher during zero field heating than during field cooling (Fig.4.2.4 b). The imaginary part dielectric response peak declines with frequency increasing in a range from 8200 for 0.1 Hz to 1100 for 1.5 kHz at field cooling (Fig.4.2.5 b) and from 14400 for 0.1 Hz to 1200 for 1.5 kHz at zero field heating (Fig.4.2.5 d).

However, there are some differences between results in experiment with field cooling (Fig.4.2.4 and Fig.4.2.5) and without additional electric field (Fig.4.2.1 and Fig.4.2.2). In the experiment with field cooling it is seen that heating curve of the permittivity's real part repeats cooling curve more accurately (Fig. 4.2.4 a compared to Fig. 4.2.1 a). Also, permittivity's real part peaks become more narrow through temperature (Fig. 4.2.5 a, c compared to Fig. 4.2.2 a, c). The imaginary part of permittivity peak has little different shape and larger amplitude difference between heating and cooling, unlikely for experiment without additional electric field (Fig.4.2.4 b compared to Fig. 4.2.1 b).

4.3 Piezoelectric Force Microscopy (PFM) measurements

PZT 1.1 Polarization Experiment

Description

During these experiments the behavior of the surface of PZT 1.1 single crystal was investigated after applying electric field to it. The polarization experiments were performed with DCP10 probe, manufactured by NT-MDT, Russia. Its parameters are tip curvature radius ~100 nm, force constant 5.5-22.5 N/m, resonant frequency 190-325 kHz (the measuring probe has 240 kHz) and tip side covered with ~100 nm doped diamond.

A relatively smooth part of the sample surface with less irregulations was chosen to make a scan. The scan size was 25 μm, called Common scan, tip velocity was 0.8 Hz with resolution speed 40 μm/s, resolution was 98 nm/px (every common scan has the same parameters). On common scan area small square pieces of 5 μm size were chosen for

polarization under electric field of different directions. Electric field was applied to the sample with tip bias during scanning small areas. After scanning with applied field for some time (usually ~15 min) the common scan was done and the changes were observed. Piezoresponse images contain 4 channels: two for out-of-plane amplitude and phase signal, called Amplitude1 and Phase1, and two for in-plane amplitude and phase signal, called Amplitude2 and Phase2.

4.3.1 Areas

During the measurements, it was recognized that the sample shows different piezoelectric response on different areas of surface, shown on figure 4.3.1.

Therefore, 3 areas with different behavior were defined:

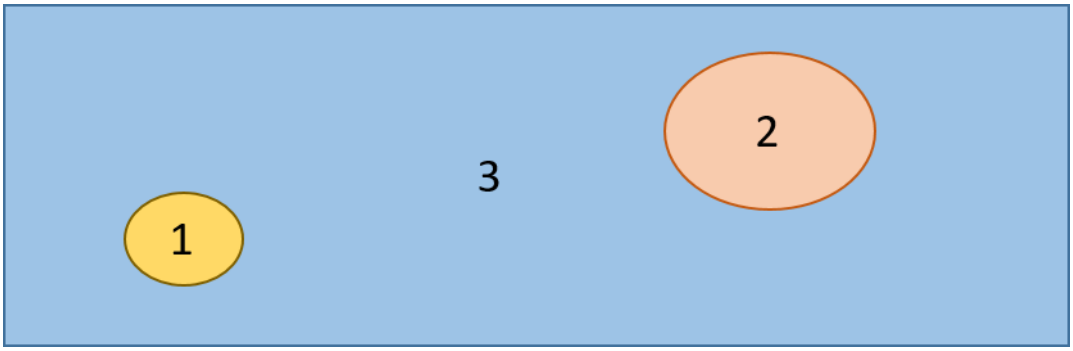

Figure 4.3.1. Scheme of PZT 1.1 sample with numbered areas showing different piezoresponse: Structural domains area (1), Changing spots area (2), Clear area with disappearing figures and no specific piezoresponse (3).

Area 1: Structural domains

Structural domains are clearly seen within low frequencies (1 kHz —50 kHz) of AC. They are clearly seen in figure 4.3.2. The domains are observed on Phase1 piezoresponse channel (Fig.4.3.2.b) with no connections with topography image (Fig.4.3.2.a). The structural domains look like sticks, usually have long narrow shape and oriented in two perpendicular directions. The pictures are stable, but sometimes they become hardly recognized during measurements. Structural domains were found only in one small area of the sample surface (Fig.4.3.1). The domains typical thickness varies in 50 – 300 nm range, their length is from 300 nm for short (perpendicular) domains to >20 µm for long (parallel) domains. The domains create a repeating pattern, where the interval between two nearest short domains is 100 – 300 nm, and between two long domains typically 2 – 5 µm (Fig.4.3.2.b).

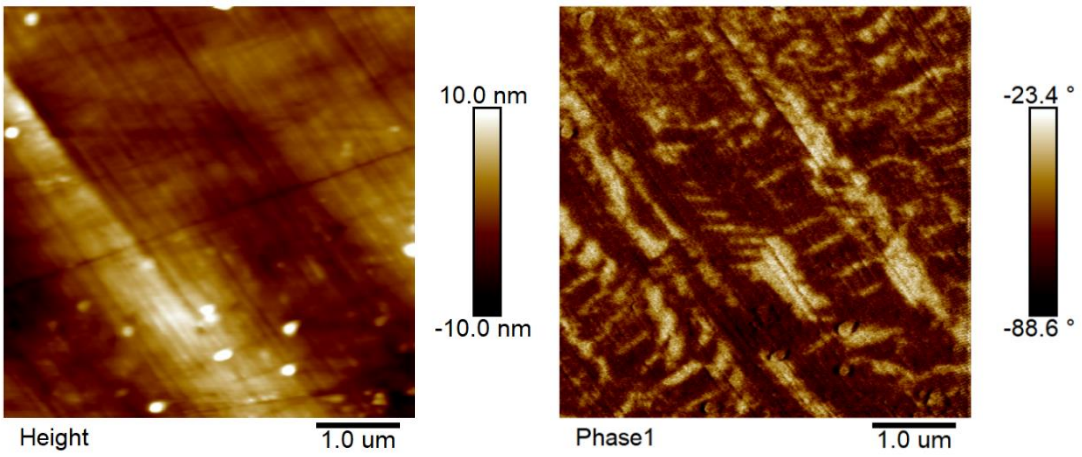

a b

Figure 4.3.2. AFM image on area of structural domains. Height and Phase1 of the scan of 5 µm size is presented in a and b, respectively.

Area 2: Changing spots

Some spots of unusual shape appeared on the surface in area 2 during measurement with resonant probe frequency. For DCP10 probes this frequency was 240-250 kHz. The shape of the spots is not constant, it appeared to depend on scan direction and applied electric field. The application of electric field did not create characteristic footprint, but changed the shape and sizes of spots significantly (Fig.4.3.3).

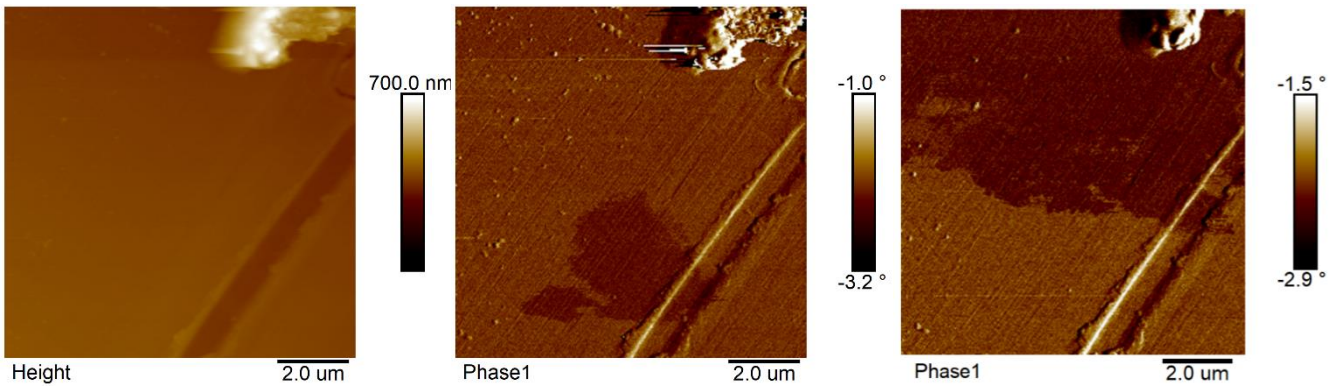

a b c

Figure 4.3.3. AFM image on area of changing spots during polarization experiment. Height of the scan of 10 µm size is presented in a, piezoresponse channel of Phase 1 scans are presented in b before polarization and c after polarization.

Area 3: Clear area

In this zone, two types of piezoresponse appear: with disappearing figures and with no specific piezoresponse. The measurements revealed different pictures that appear only once or repeated but suddenly disappear with very small changes in scan parameters like

scan size. They look like lines, spots and scratches and are not related to topography (Fig.4.3.4). Such behavior of PZT single-crystals has not been noted in the literature earlier.

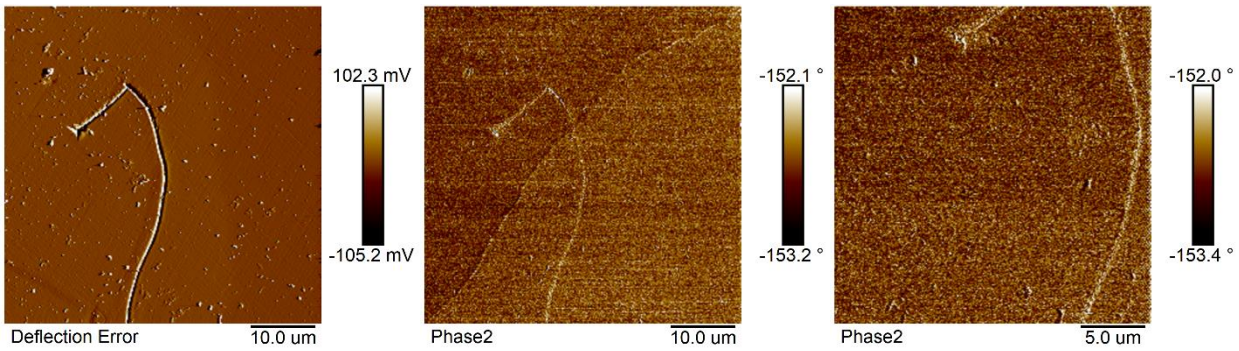

a b c

Figure 4.3.4. AFM image on area of disappearing figures. Deflection Error of the scan of 50 µm size is presented in a, piezoresponse channel of Phase 2 scans are presented in b, where appears diagonal line not connected to topography, and c after changing scan size to 25 µm, where line disappeared.

For Phase2 (piezoresponse channel in Fig. 4.3.4 b) the diagonal line can be recognized from left down corner to right up corner. It crosses the mechanical scratch, which is seen on all images. There is no such line on Deflection Error scan (Fig. 4.3.4 a), which characterizes the topography of the sample surface. Also, the line is not seen after zoom (Fig. 4.3.4 c) for same Phase2 channel, as it should. Such behavior could appear because of measurement features.

Most parts of the surface did not show any response on any measured AC frequencies. However, they have footprint after applying electric field that lasts for some time, usually about an hour. Additionally, there was common behavior for the sample that piezoresponse pictures get weaker during measurements.

According to the measurements seen on figures 4.3.2 — 4.3.4 the sample can be considered inhomogeneous. Perhaps it has some grains with different stoichiometry.

4.3.2 Polarization of structural domains

Structural domains were found in small area near the corner of the sample (Area 1 in figure 4.3.1). The domains are usually seen in a range of frequencies from 1 kHz to 50 kHz. This experiment was performed with 30 kHz AC and 10 V amplitude. The scans taken during this experiment are shown on figure 4.3.5.

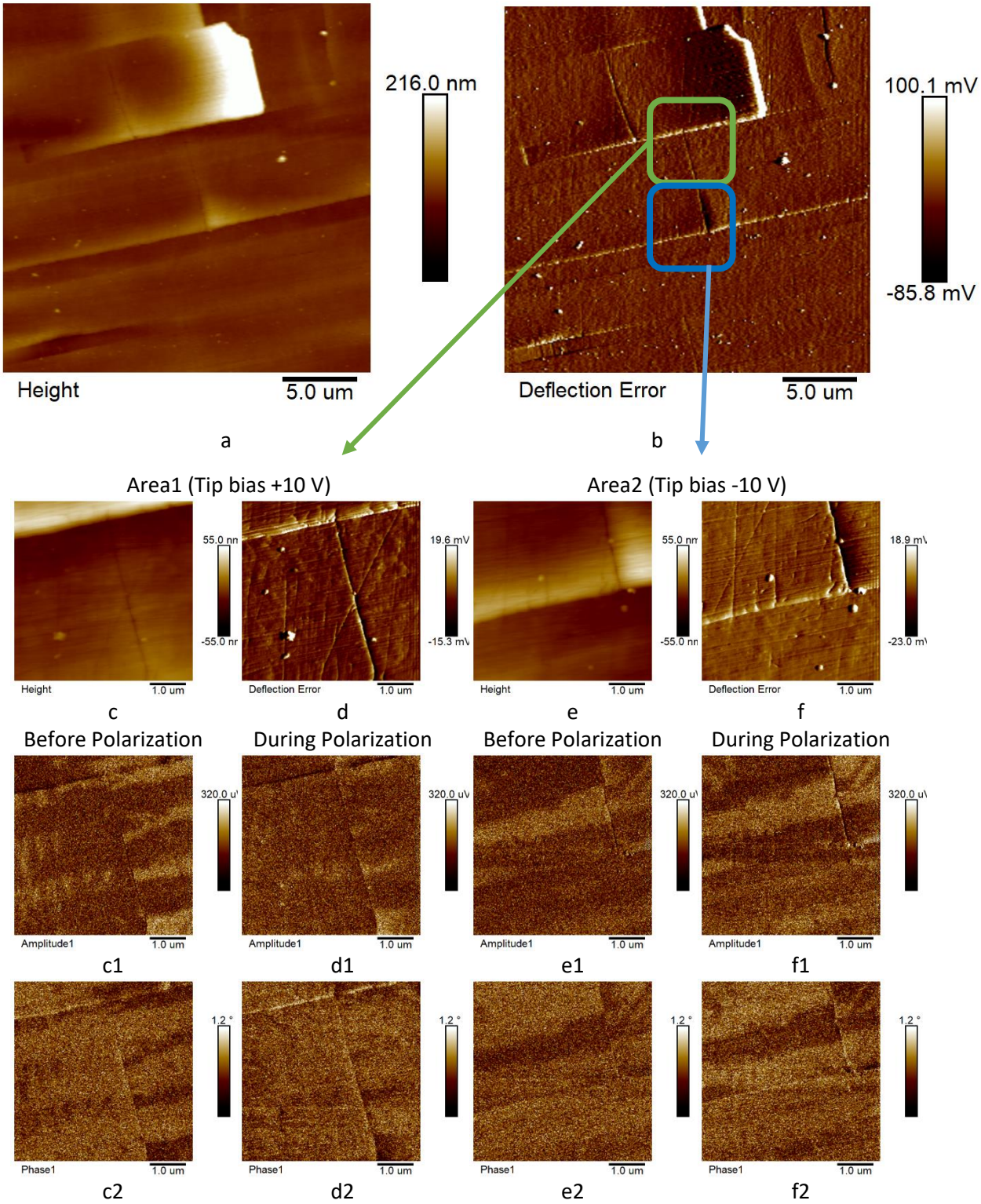

Figure 4.3.5. AFM image of polarization experiment on area of structural domains. Height and Deflection error of common scan of 25 µm size is presented on a and b, respectively. The chosen areas of 5 µm are marked with green and blue square frames on b. The Topography and Deflection error of chosen area 1 (c, d, respectively). Piezoresponse images on area 1 before polarization and during polarization c1-c2 and d1-d2, respectively. The Topography and Deflection error of chosen area 2 (e and f, respectively). Piezoresponse images on area 2 before polarization and during polarization e1-e2 and f1-f2, respectively.

Two areas were chosen for polarization (Fig.4.3.5 b, green frame for +10 V polarization and blue frame for -10 V polarization). One under another in the center of common scan. Firstly, upper area was polarized under +10 V for ~15 min (first polarization), the common scan was performed, then down area was polarized under -10 V for ~15 min (second polarization) and the common scan was repeated again. As seen in figures of 5 µm scans (Fig.4.3.5 c1-f1 and c2-f2), positive voltage made piezoresponse picture more blurred and negative voltage made it clearer. The piezoresponse (Amplitude1 and Phase1) on all common scans of 25 µm size within time frame of the experiment is shown in the table 4.3.1. The Height and Deflection Error images remained similar during whole experiment. They are presented in figure 4.3.5 (a) and (b).

Table 4.3.1. AFM images of polarization experiment on the area of structural domains for out-of-plane channels. All scan sizes are 25 µm.

Before Polarization	After first Polarization (+10 V for ~15 min)	After second Polarization (-10 V for ~15 min)	After both Polarization (~100 min after first polarization and ~65 min after second polarization)
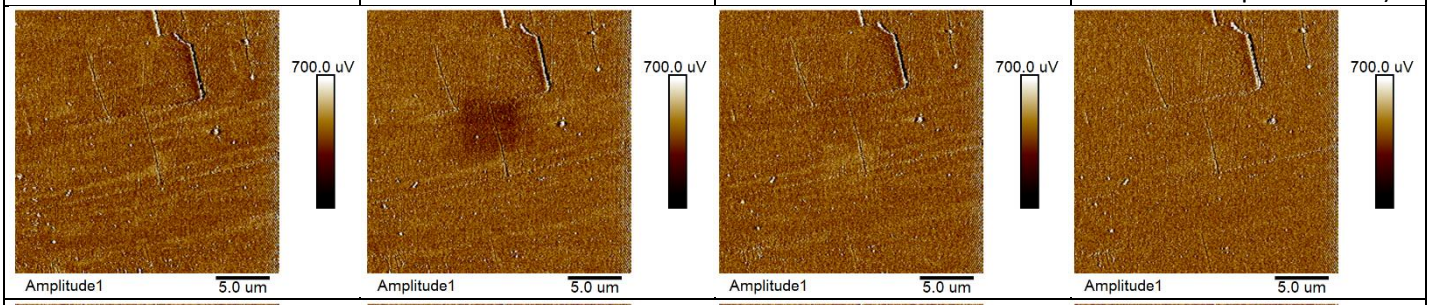			
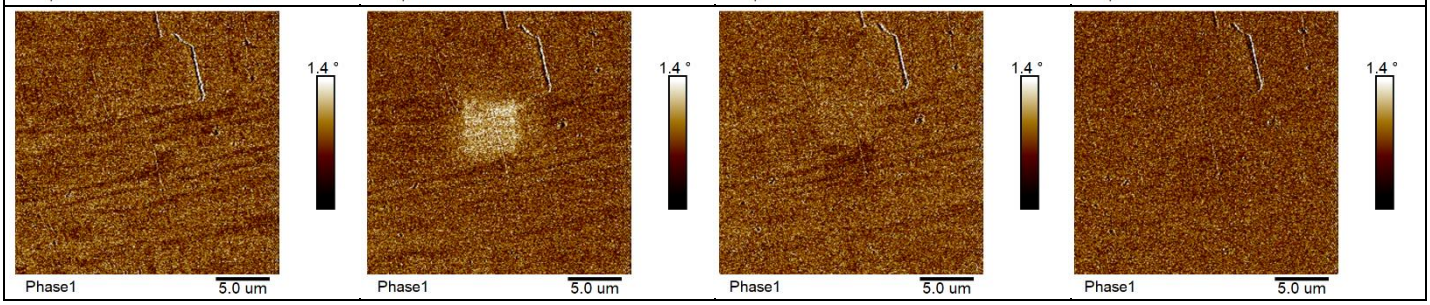			

Both positive and negative polarization scans left footprints of opposite “colors”. That means the piezoresponse intensity of polarized areas has changed. For out-of-plane amplitude positive bias decreased the signal and negative increased it. For out-of-plane phase signal the opposite is true. The in-plane piezoresponse images showed very weak footprint, so they were not presented. Moreover, we saw that both polarization footprint and structural domains picture became weaker with time. In our experiment it took about

1 hour to erase the footprint of ~15 min -10 V bias and ~100 min to erase the footprint of ~15 min +10 V bias.

A bit different place in the same area was chosen. The piezoresponse after applying ±10 V and ±5 V electric field (Fig.4.3.6) was measured. The result of this experiment is shown in the tables 4.3.2 and 4.3.3 for amplitude and phase respectively.

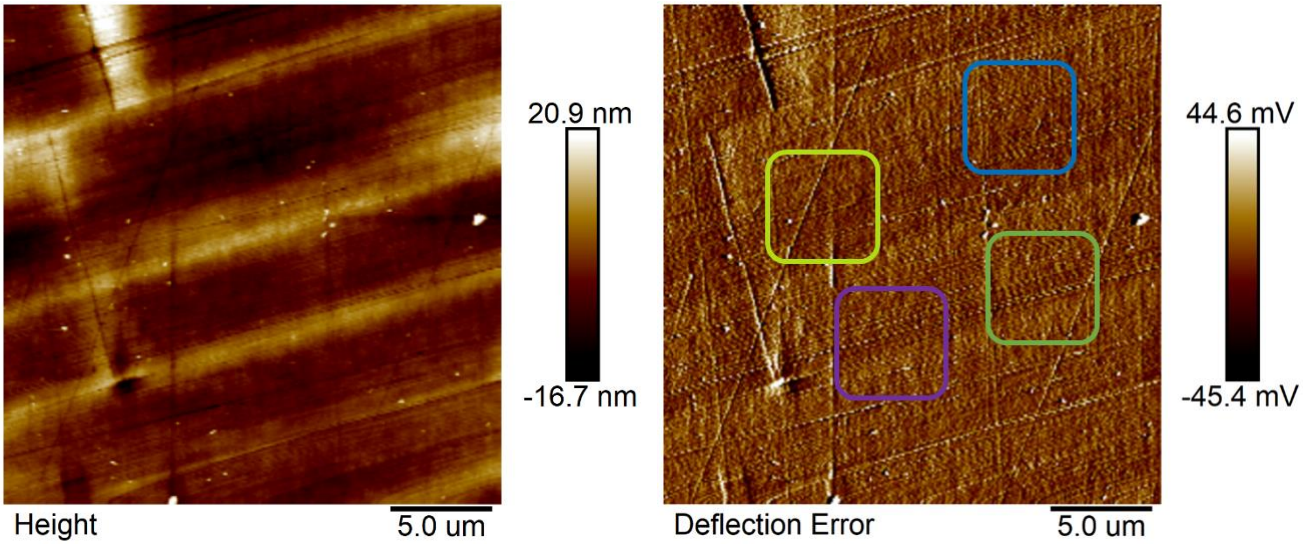

a b

Figure 4.3.6. AFM images of Height (a) and Deflection error (b) of the scanned area with size 25 µm. The polarized smaller areas are marked with frames in accordance to polarization. Green frame (area 3): polarization with +10 V, blue frame (area 4): polarization with -10 V, lemon frame (area 1): polarization with +5 V, purple frame (area 2): polarization with -5 V

The method of experiment is described above. It is seen from the tables that the piezoelectric response behavior is the same as it was for the previous area. Just like earlier, the polarization footprint under negative voltage was much weaker than under positive voltage. Furthermore, for this area the footprint appeared also after polarization with smaller bias. The contrast between footprints and background removed quite quickly after removing the bias.

Table 4.3.2. AFM images of polarization experiment on the area of structural domains for Amplitude1 channel. Firstly, polarization was made with +5 V and -5 V tip bias, then with +10 V and -10 V. All scan sizes are 25 µm.

Before Polarization	After Polarization on area1 (+5 V for ~15 min)	After Polarization on area2 (-5 V for ~15 min)
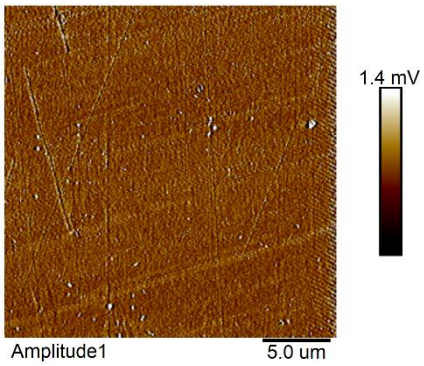	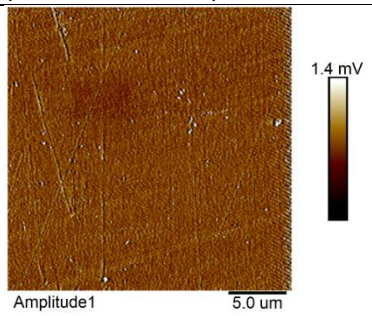	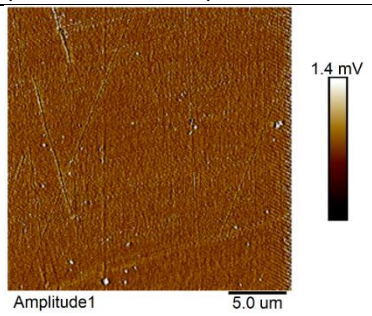
	After Polarization on area3 (+10 V for ~15 min)	After Polarization on area4 (-10 V for ~15 min)
	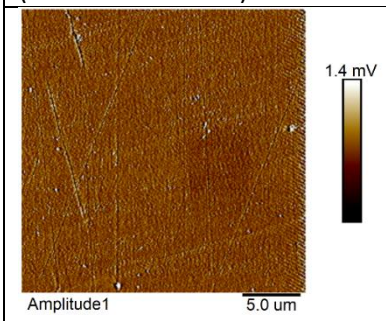	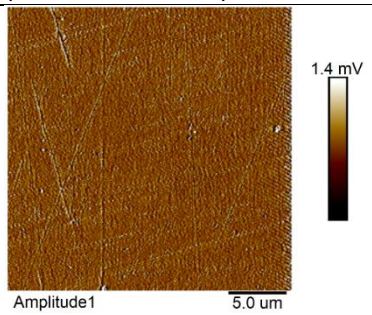

Table 4.3.3. AFM images of polarization experiment on the area of structural domains for Phase1 channel. Firstly, polarization was made with +5 V and -5 V tip bias, then with +10 V and -10 V. All scan sizes are 25 µm.

Before Polarization	After Polarization on area1 (+5 V for ~15 min)	After Polarization on area2 (-5 V for ~15 min)
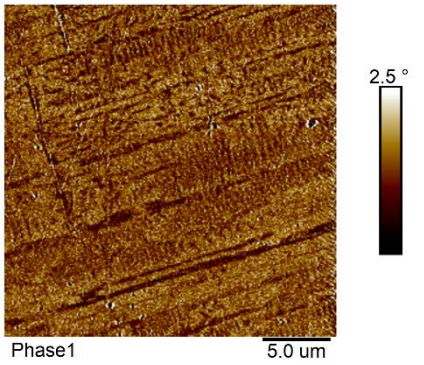	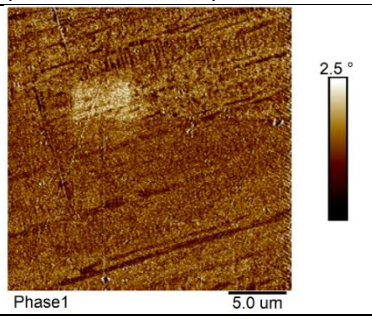	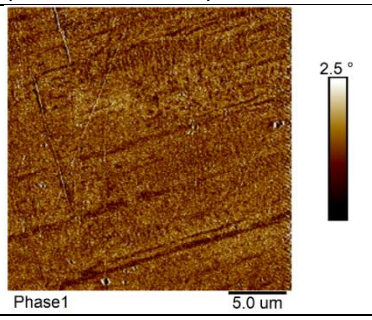
	After Polarization on area3 (+10 V for ~15 min)	After Polarization on area4 (-10 V for ~15 min)
	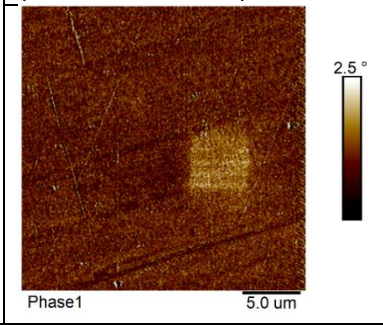	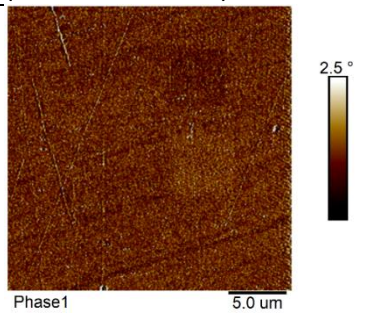

4.3.3 Polarization of Clear area

Piezoresponse signal was not visible with all measured frequencies in areas different from area 1 and 2 (Fig. 4.3.1). Amplitude and Phase channels showed only topography features. This part of surface was investigated with 240 kHz and 30 kHz AC (Fig.4.3.7 and Fig.4.3.8 respectively).

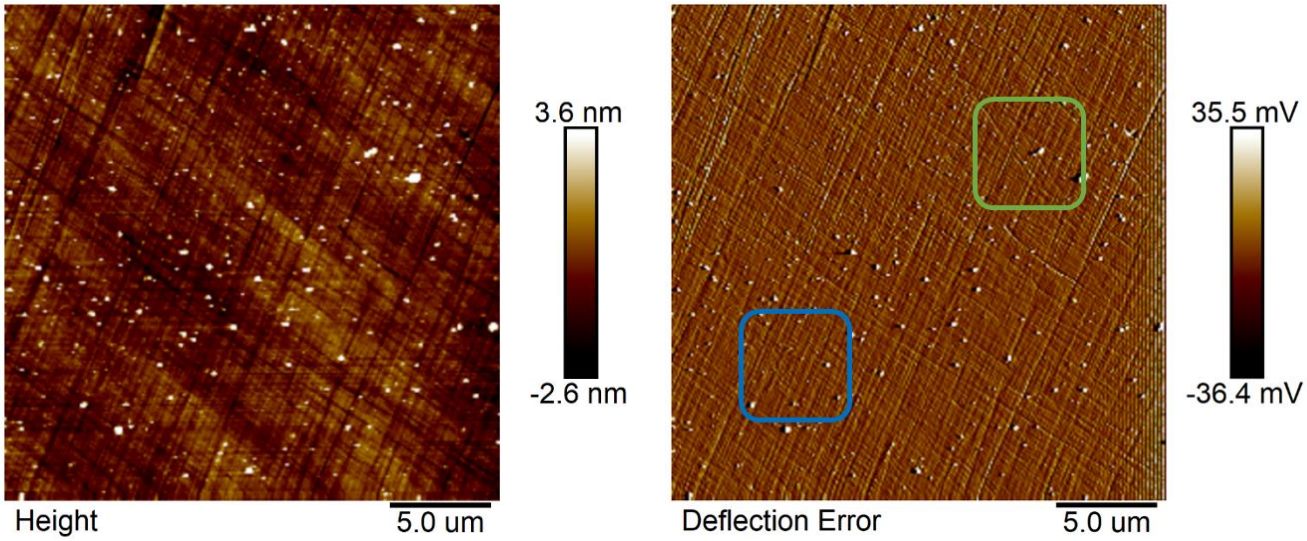

a b

Figure 4.3.7. AFM images of Height (a) and Deflection error (b) of the clear area scans with size 25 µm. The polarized smaller areas are marked with frames in accordance with polarization, measured with 240 kHz AC frequency. Green frame: polarization with +10 V, blue frame: polarization with - 10 V

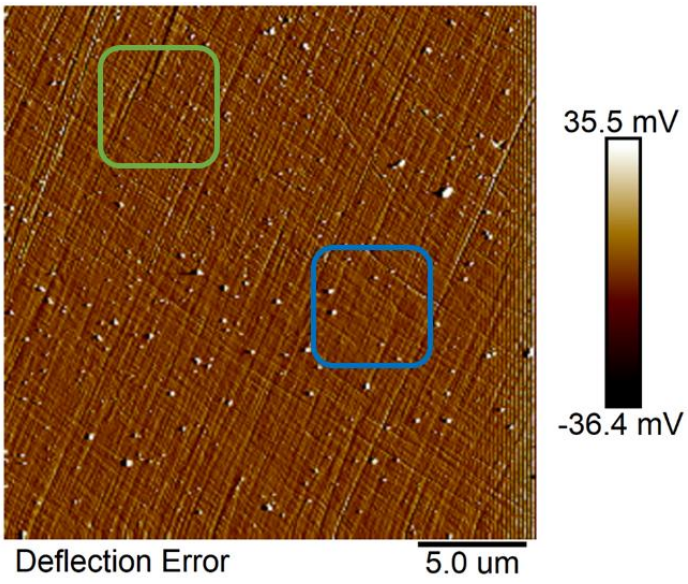

Figure 4.3.8. AFM image of Deflection error of the previous scanned area with size 25 µm. The polarized smaller areas are marked with frames in accordance to polarization, measured with 30 kHz AC frequency. Green frame: polarization with +10 V, blue frame: polarization with -10 V

Sometimes there appeared different figures like lines and scratches, but they suddenly disappeared without changing interaction. The 240 kHz AC was used, as it is the tip resonance frequency, and 30 kHz AC was used, as it provided the clearest piezoresponse pictures.

Firstly, the experiment was provided with 240 kHz AC frequency, represented in table 4.3.4. Then the same experiment was provided with 30 kHz AC frequency, represented in table 4.3.5.

Table 4.3.4. AFM images of polarization experiment on clear area for piezoresponse out-of-plane channels, measured with 240 kHz AC. Polarization was made with +10 V and -10 V tip bias. All scan sizes are 25 µm

Before Polarization	After first Polarization (+10 V for ~15 min)	After second Polarization (-10 V for ~15 min)
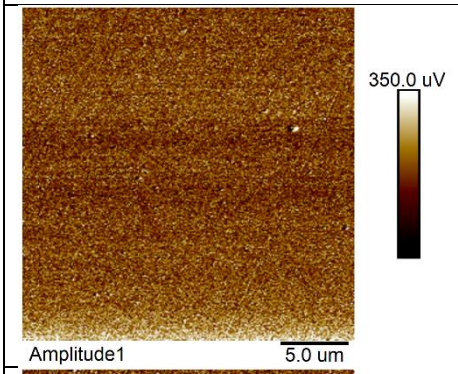	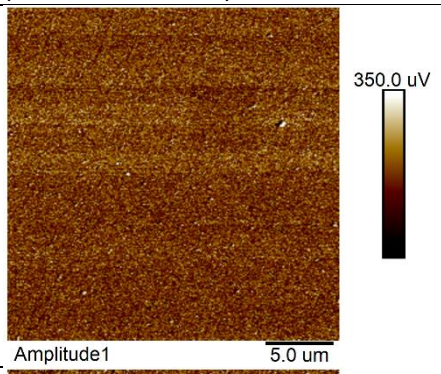	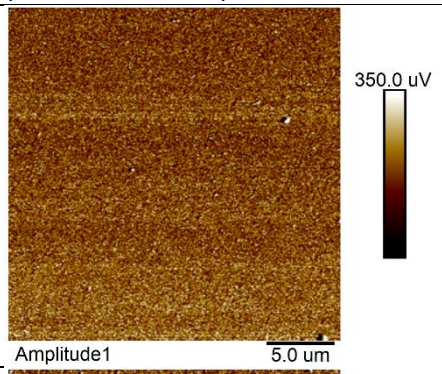
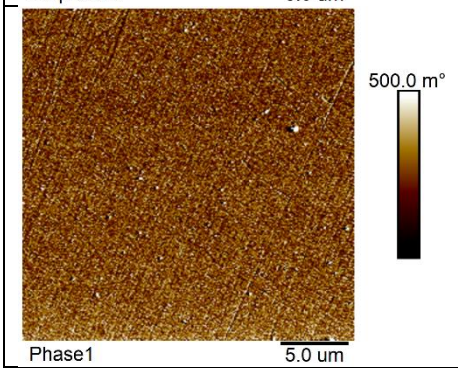	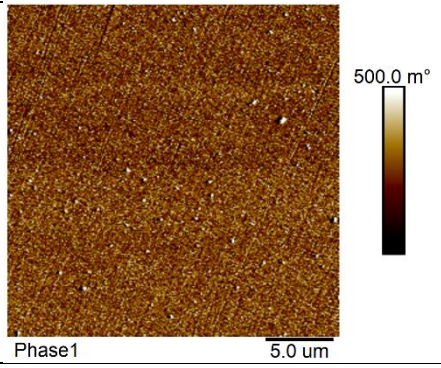	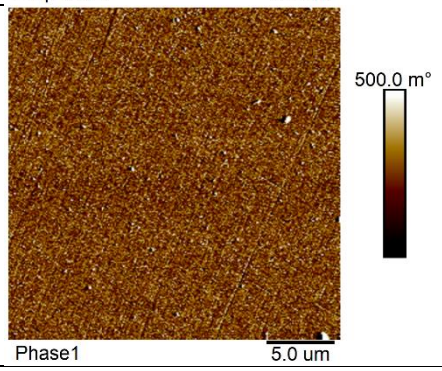

Table 4.3.5. AFM images of polarization experiment on clear area for piezoresponse out-of-plane channels, measured with 30 kHz AC. Polarization was made with +10 V and -10 V tip bias. All scan sizes are 25 µm

Before Polarization	After first Polarization (+10 V for ~15 min)	After second Polarization (-10 V for ~15 min)
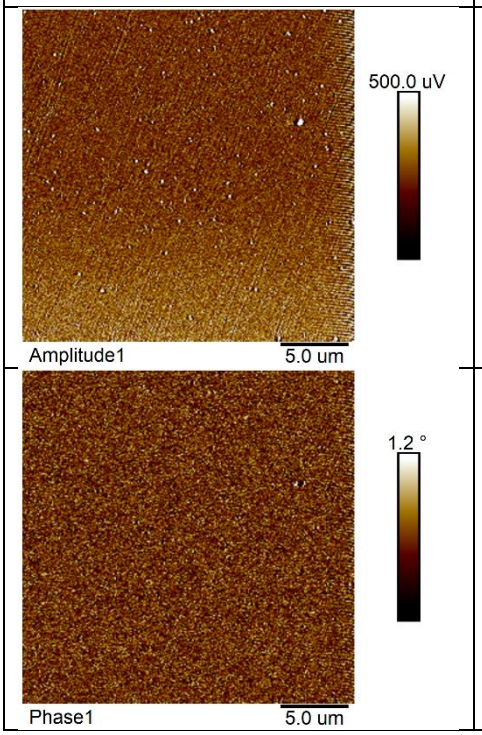	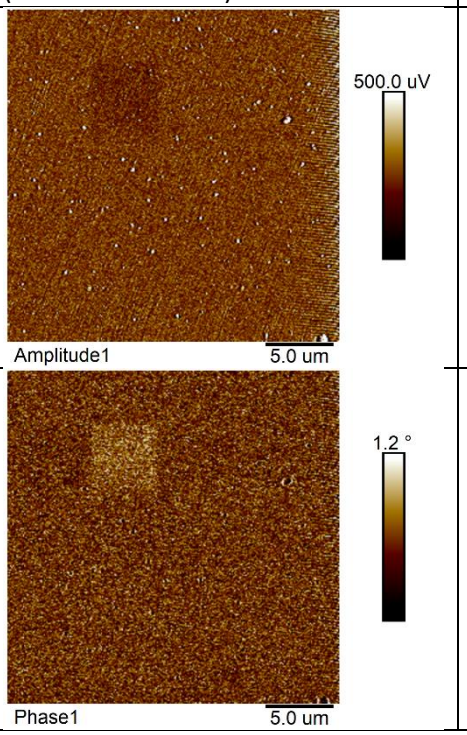	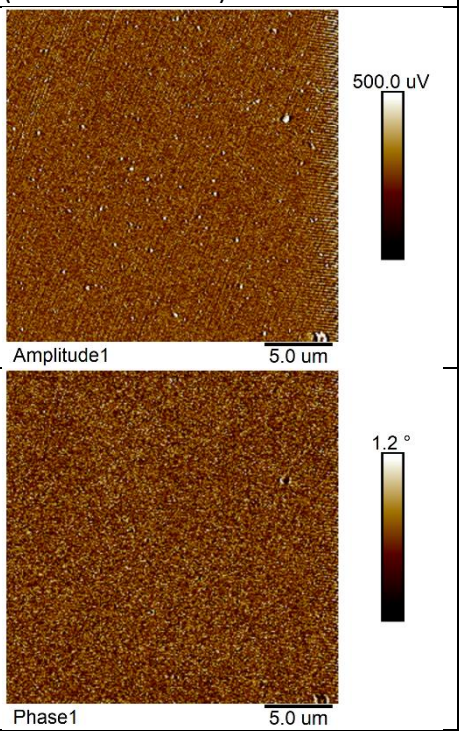

It is visible that footprint appeared after applying +10 V and did not appear after applying -10 V. The piezoresponse images were almost the same for both 240 kHz and 30 kHz measured frequencies, but the picture was noisier with higher frequency. Although the probe resonance frequency is preferable for piezoelectric measurements, in this case it showed less clear picture than at lower frequency.

4.3.4 Polarization of changing spots area

Some spots changing during up and down scan direction were found on the surface. The topography images are represented in Fig. 4.3.9, and piezoresponse images for both out-of-plane and in-plane response channels are represented in table 4.3.6. Measurement was performed with probe resonance frequency 240 kHz. Scan size was 10 µm of the same place at sample.

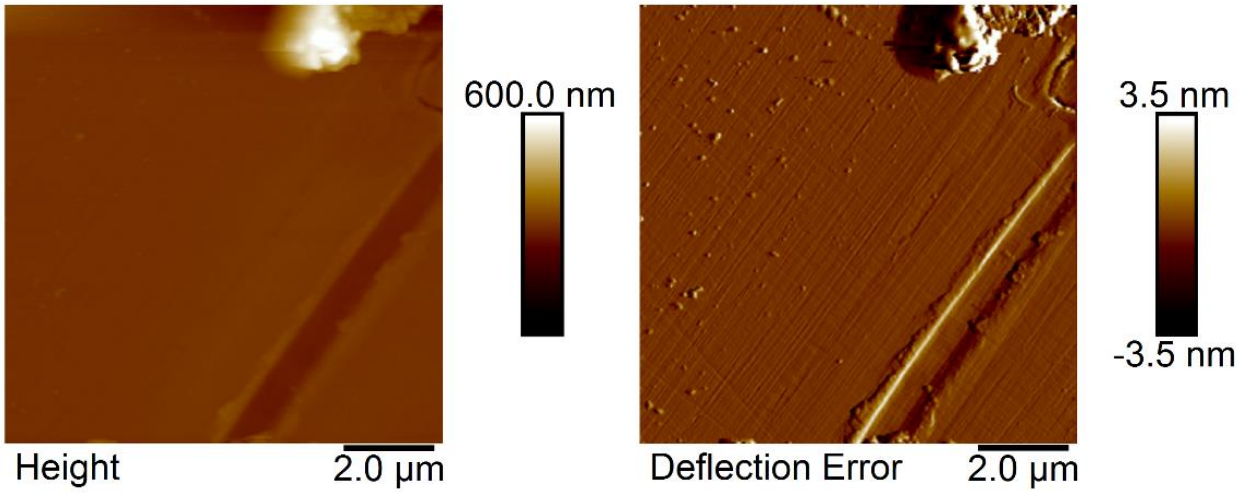

a b

Figure 4.3.9. AFM images of Height (a) and Deflection error (b) on the area of changing spots, scan size 10 µm.

Table 4.3.6. AFM images of the changing spots area for all piezoresponse channels, after down and up scan direction. Scan sizes are 10 µm, measured frequency is 240 kHz AC.

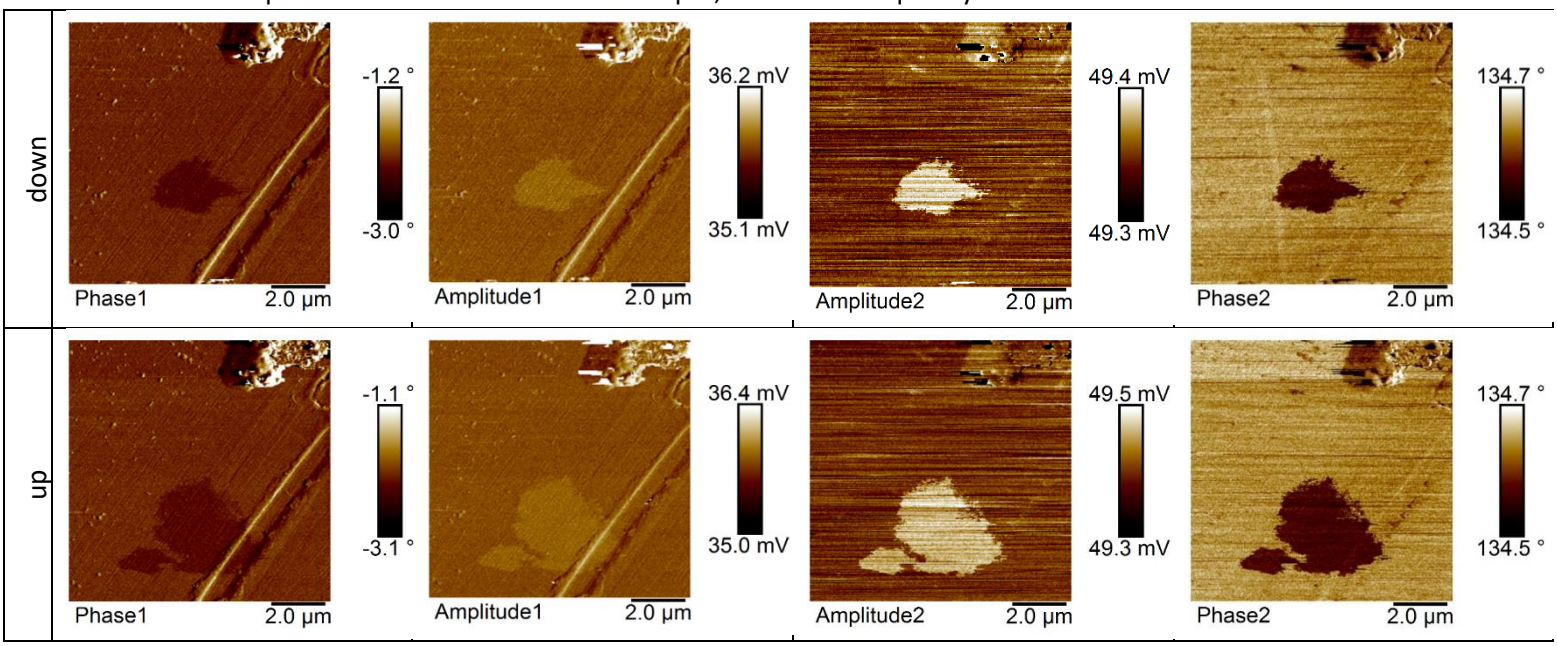

The table 4.3.6 shows that all piezoresponse channels show the same spot for the scan. The shape of the spot was a bit different with scan direction (for up and down scans), so we marked both spots on the Phase1 scan, represented in figure 4.3.10. It is visible that piezoresponse patterns look very differently from patterns of previous ones (structural domains area, e.g. Fig.4.3.2). That means the domains reaction of the surface have different nature, what should be investigated further.

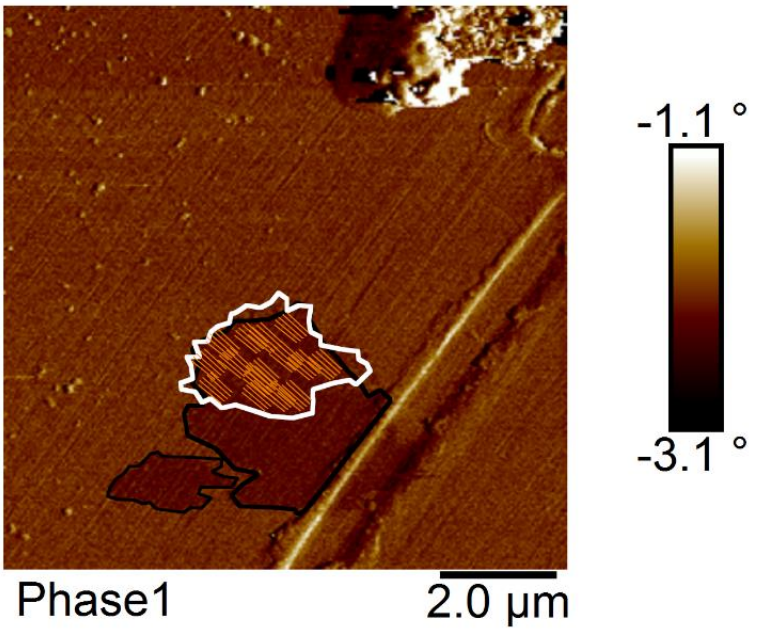

Figure 4.3.10. AFM image of the changing spots area for out-of-plane phase channel after up scan direction, with marked spots after down and up scan direction. Black frame shows spot for up scan direction, white frame shows for down scan direction; orange dashed area is common for both. Scan size is 10 µm.

Then polarization experiment was performed for the same area (Fig.4.3.11). The results are shown in table 4.3.7.

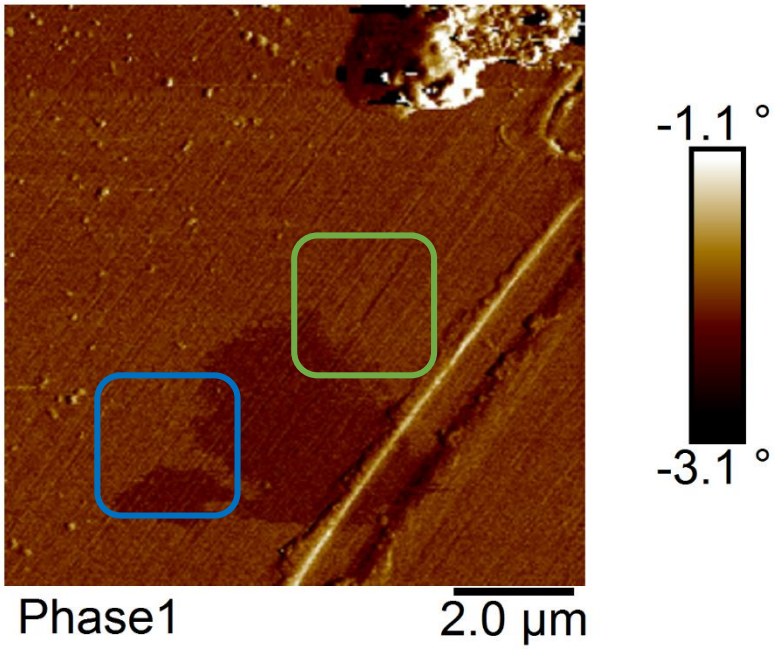

Figure 4.3.11. AFM image of Phase1 on common scan of changing spots area with size 10 µm. The polarized smaller areas are marked with frames in accordance with polarization. Green frame: polarization with +10 V, blue frame: polarization with -10 V.

At common, 10 µm scan size area a small area with size of 3 µm was chosen and polarized with Tip Bias +10 V for ~10 min. (All 3 µm scans during polarization are not added as these images do not have any information). Then common scan was done, after that another 3 µm area was polarized in the same way under opposite field. The scan areas were chosen to see the reaction of both light and dark piezoresponse domains on electric polarization.

Table 4.3.7. AFM images of polarization experiment on the changing spots area for piezoresponse Amplitude1, Phase1 and Phase2 channels, measured with 240 kHz AC. Polarization was made with +10 V and -10 V tip bias. All scan sizes are 25 µm.

Before Polarization, spot 1	After first Polarization, spot 2 (+10 V for ~15 min)	After second Polarization, spot 3 (-10 V for ~15 min)
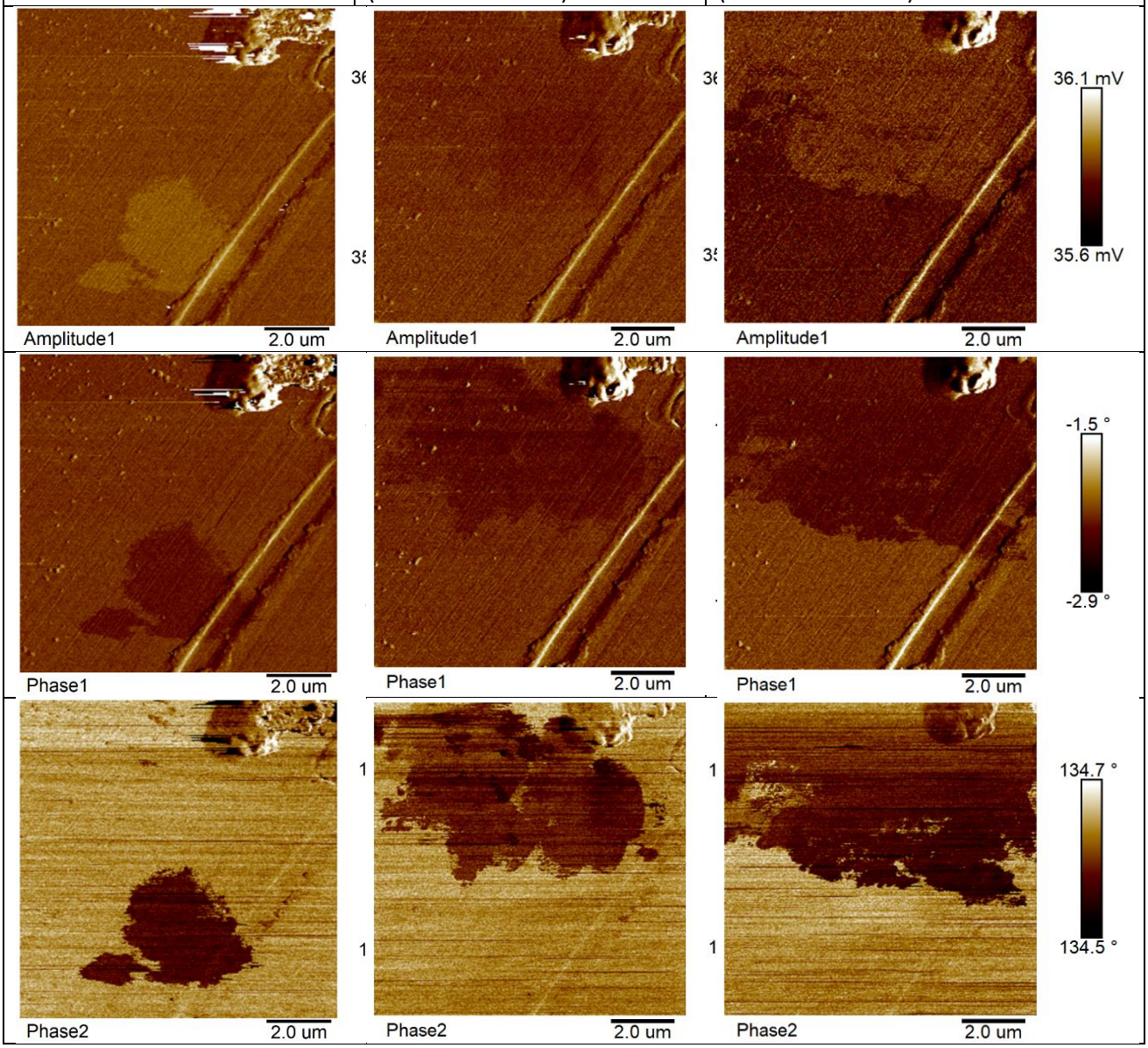		

After applying Tip Bias +10 V the picture changed dramatically. Footprint from polarization was slightly recognized in Amplitude1 channel. However, the footprint disappeared quickly (<5 min, the time required for 1 scan). Small dark spots, visible in the first column turned to light and another dark spot appeared (second column). So, an assumption can be made that electric field application stimulates the sample to create or change its own domains.

After applying -10 V the spots became bigger. The scan size was enlarged to 50 µm to see whole spots (Fig.4.3.12). However, it did not work. The piezoresponse was not registered. Changing scan size back to 10 µm provided no response.

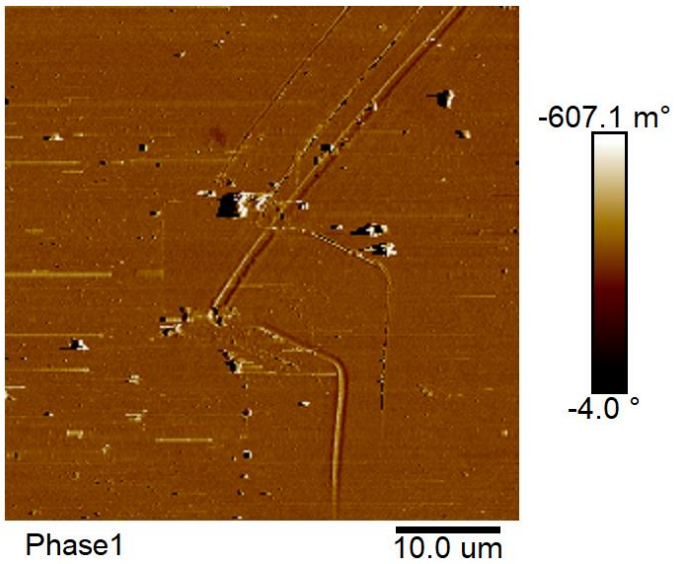

Figure 4.3.12. AFM image of Phase1 on the same as previous scan area of changing spots, with scan size 50 µm.

Then other place on the surface was chosen and polarized. The result is represented in Fig. 4.3.13. Big spots were again visible. Therefore, scanning started with 10 µm scan size (Fig.4.3.13 a, b), then enlarged to 25 µm size (Fig.4.3.13 c, d). There the whole spot was observed. The measurements were repeated every 10 minutes. In the Fig. 4.3.14 the spot changing is clearly seen (also it could be that the spot became smaller through time or during measurements).

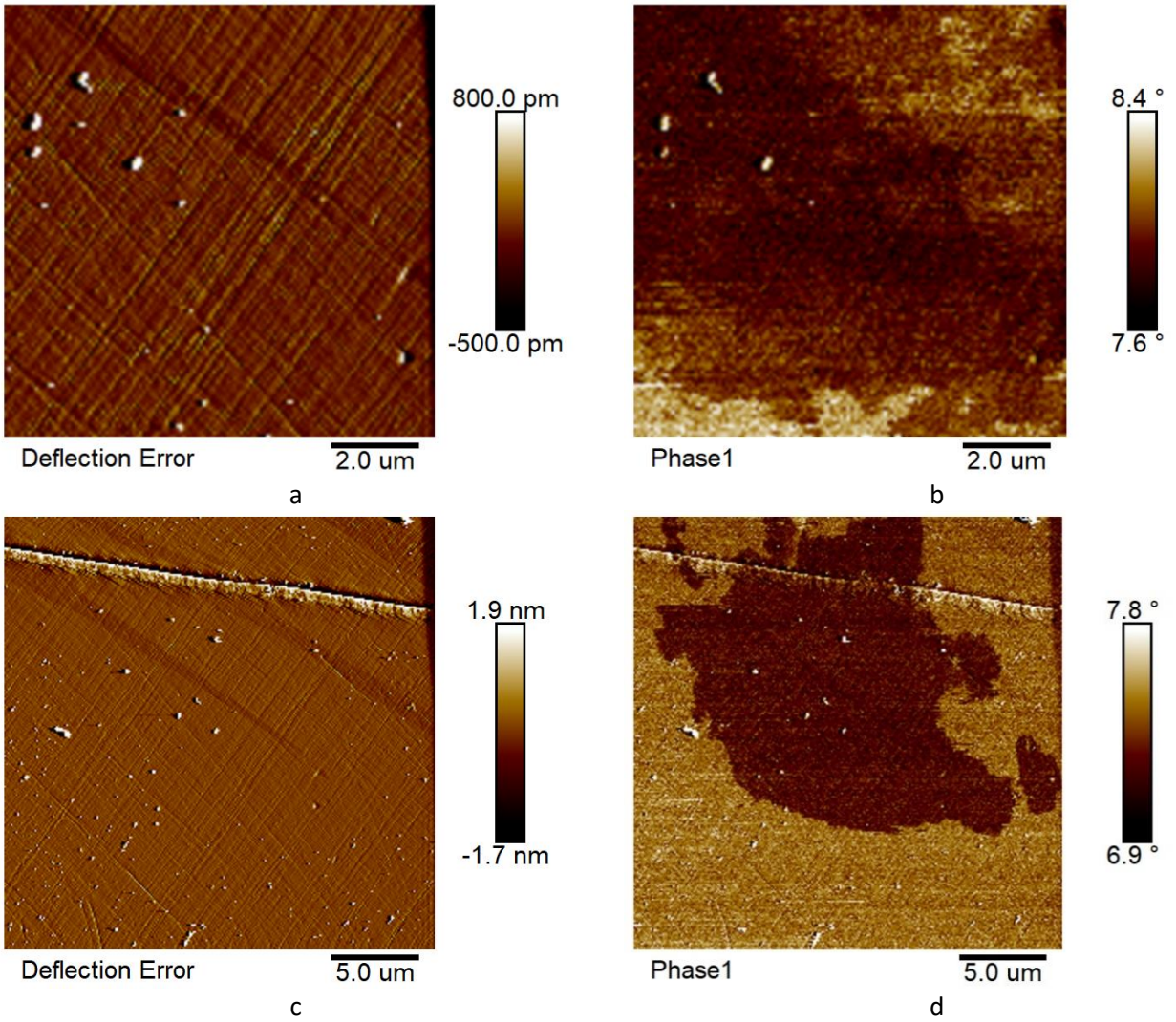

Figure 4.3.13. AFM image of Deflection Error (a),(c) and Phase1 (b),(d) on the changing spots area after polarization, with scan size 10 µm (a),(b) and 25 µm (c),(d).

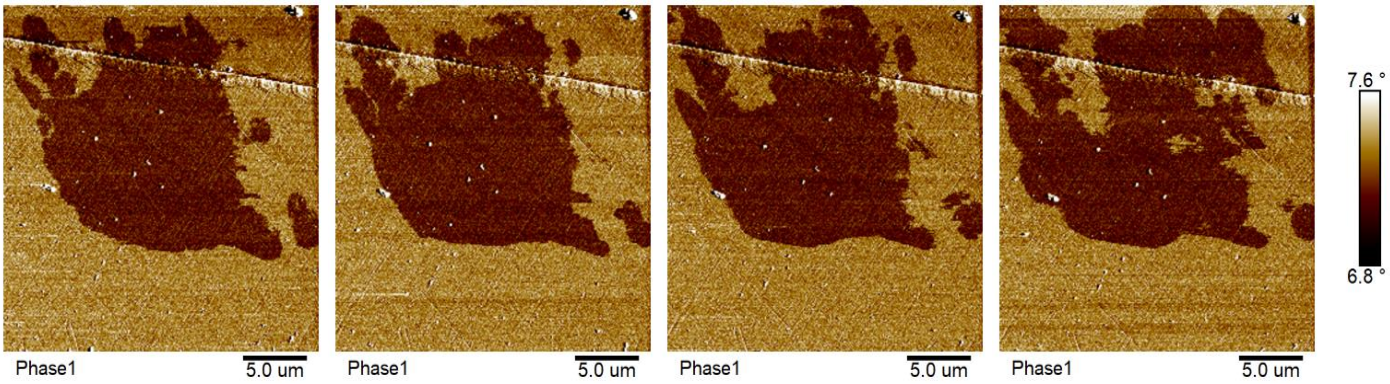

Figure 4.3.14. AFM image of Phase1 on the changing spots area after polarization, with scan size 25 µm through time. The time delay between two nearest scans was ~10 min.

4.3.5 PMN PT20

The experiments were made with PMN PT20 sample. Firstly, we scanned surface using different frequencies to find piezoresponse picture. With SCM-PIT probe at low frequencies (<20 kHz) some spots were found. The probe parameters were tip curvature radius 25 nm, force constant 2.8 N/m, resonant frequency 75 kHz and tip side covered with conductive PtIr (manufacturer Bruker, USA). The topography and piezoresponse of investigated area shown on figure 4.3.15. The measurement was done with 10 kHz frequency and 6 V AC amplitude and scan size 10 µm. The scan parameters were tip velocity 1 Hz and resolution 26 nm/px.

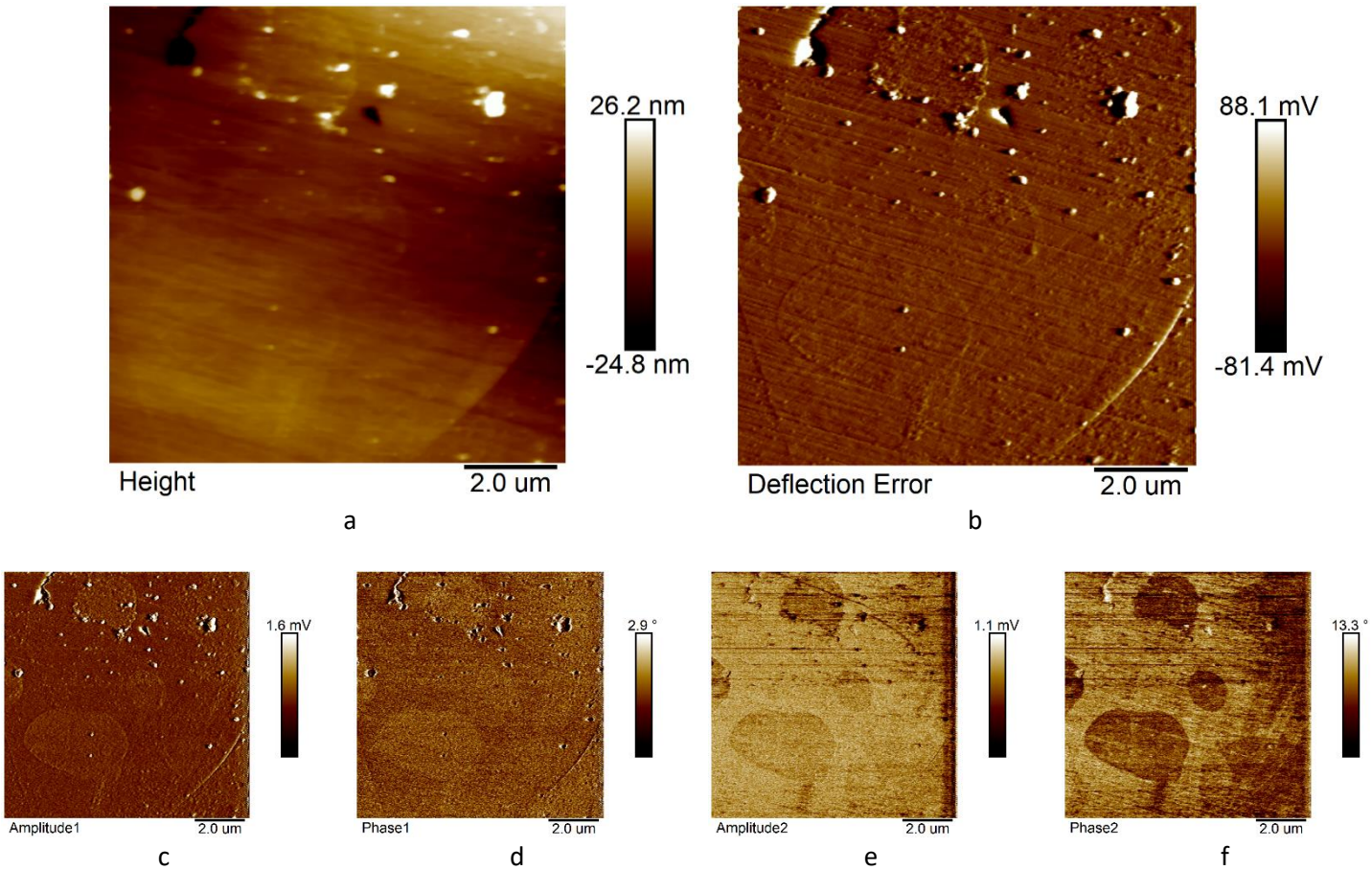

Figure 4.3.15. AFM images of the surface part of PMN PT20 ceramic sample. Scan size is 10 µm, topography scans contain Height (a) and Deflection Error (b); piezoresponse scans contain out-of-plane amplitude (c) and phase (d), in-plane amplitude (e) and phase (f).

Several round spots are visible in all piezoresponse channels. The radius of the spots varies from 0.8 µm to 2 µm. The pattern did not change for either up or down scan

directions and did not depend on time. They could be seen on few frequencies and AC amplitudes. Such piezoresponse picture was found only in one sample area.

Polarization experiment

Polarization experiments were performed with PMN PT20 sample. The method of the experiment has been described above. The same DCP10 probe as for PZT experiments was used for measurements. The measurements for this and the next experiment were made for 50 kHz frequency and 10 V AC amplitude.

The experiment shown in Fig. 4.3.16 was performed at the central part of the sample. At 25 µm common scan area several 5 µm areas were chosen for polarization under ±10 V, ±5 V. After polarization common scans were repeated and the next scan was made after quite long period of time (~1-2 hours). Then common scans were made after polarization of small areas under ±1 V. The piezoresponse scans are shown in the table 4.3.8.

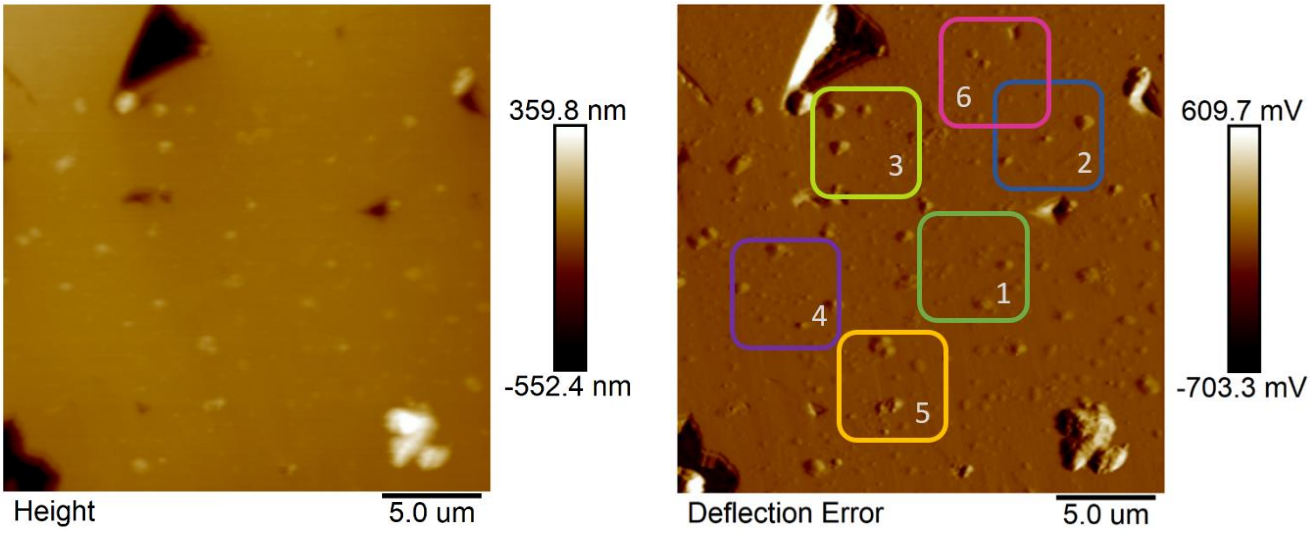

Figure 4.3.16. AFM images of Height (a) and Deflection Error (b) common scan of central part of PMN PT20 sample. On Deflection Error image polarization areas are marked: 1,3,5 are under +10,+5,+1 V respectively and 2,4,6 are under -10,-5,-1 V respectively

It is seen that all piezoresponse channels show not smooth pictures. These pictures create some pattern. Additionally, both positive and negative voltages lead to the same footprints with different intensities. It is seen that negative voltage gave stronger footprint than positive voltage. Application of higher voltage created clearer and stronger footprint that lasts for a long time (~ 1 hour).

Table 4.3.8. AFM piezoresponse images of out-of-plane amplitude and phase (Amplitude1, Phase1), in-plane amplitude and phase (Amplitude2, Phase2) during polarization experiment; scan size 25 µm.

	Out-of-plane amplitude	Out-of-plane phase	In-plane amplitude	In-plane phase
Before Polarization	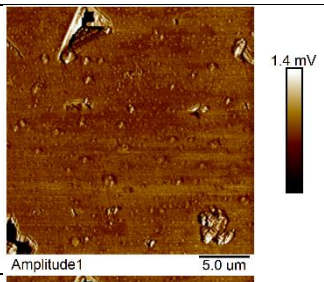	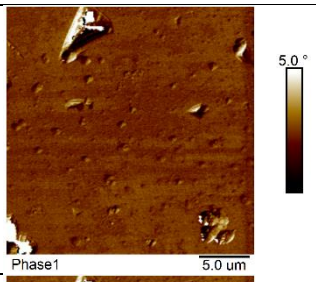	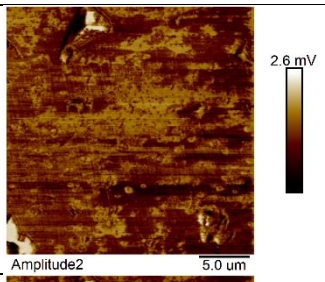	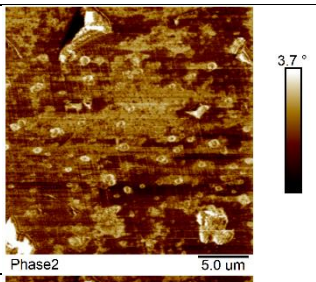
After Polarization on area1 (+10 V for 15 min)	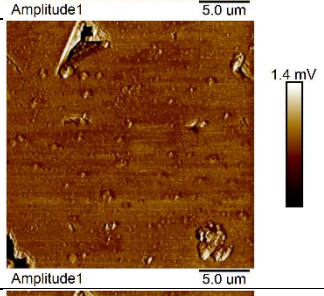	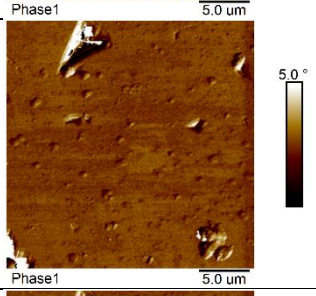	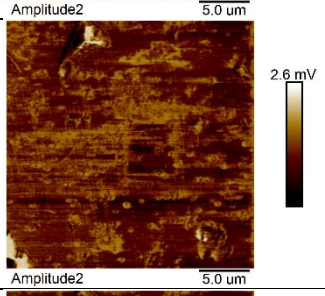	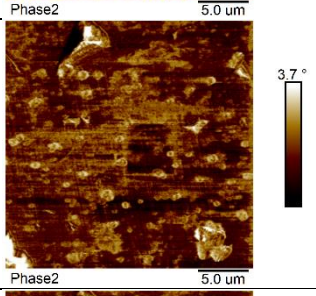
After Polarization on area2 (-10 V for 15 min)	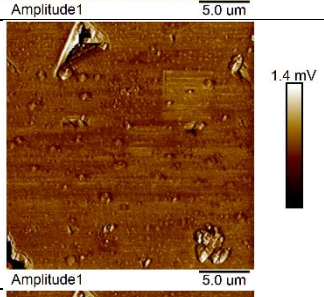	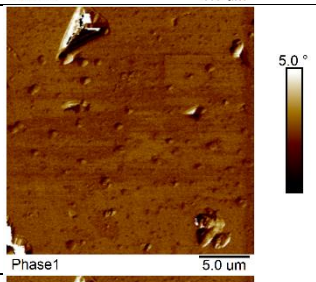	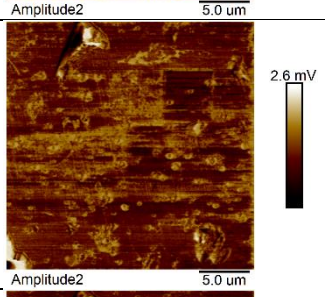	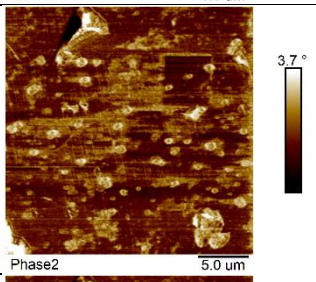
After Polarization on area3 (+5 V for 15 min)	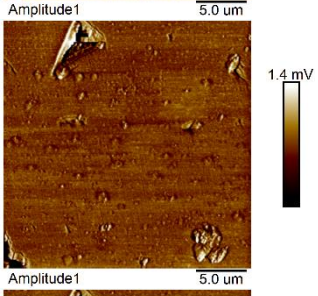	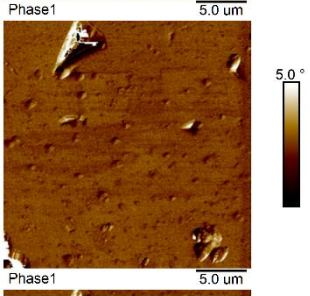	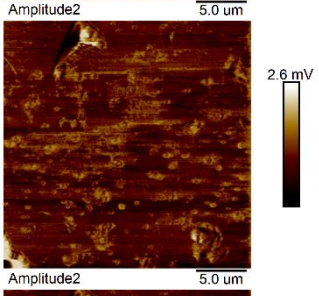	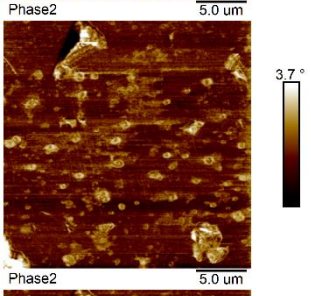
After Polarization on area4 (-5 V for 15 min)	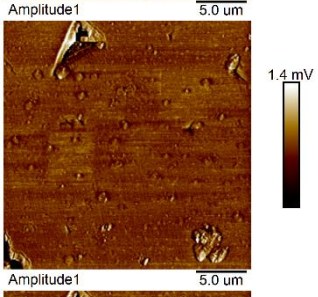	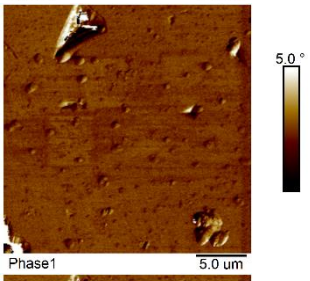	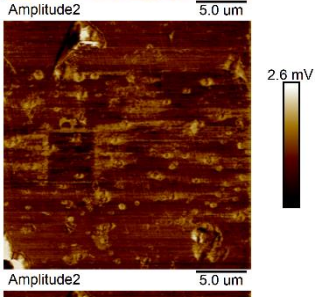	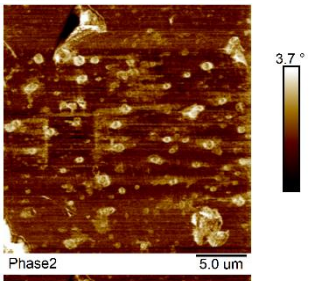
After 1 hour	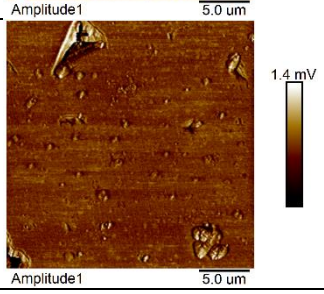	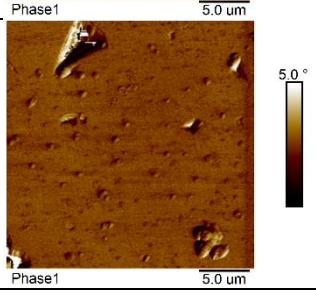	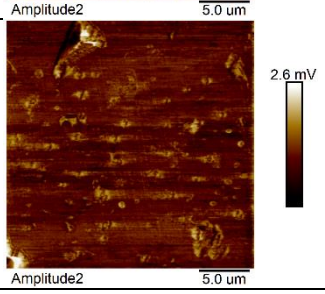	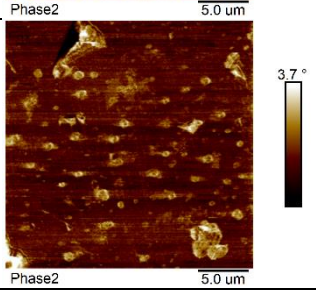

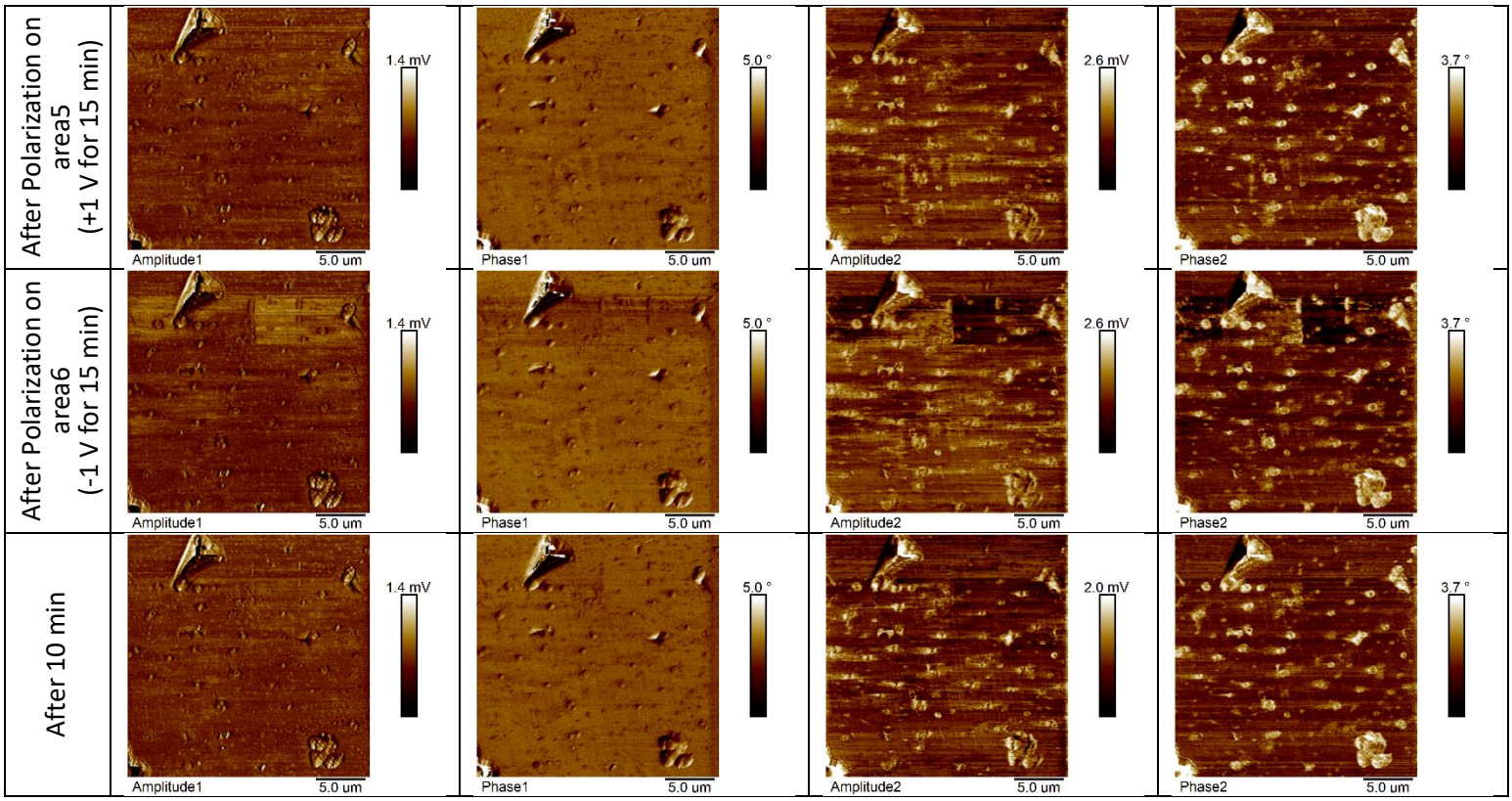

The footprint is seen in all piezoresponse channels. Before polarization the piezoresponse picture did not change with time. After all applied voltages the footprint could be recognized. Positive and negative applied voltage polarized the sample surface in one direction. This could mean the existence of some initial electric on the surface.

Next was investigated another part of the sample, which was close to sputtered electrode. The topography is shown in Fig. 4.3.17.

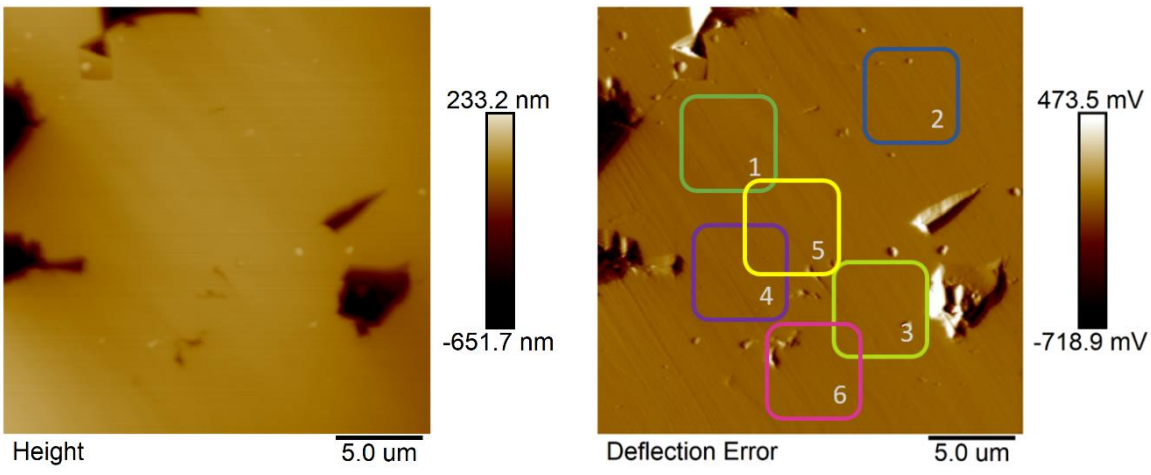

Figure 4.3.17. AFM images of Height (a) and Deflection Error (b) common scan for near to sputtered electrode part of PMN PT20 sample. On Deflection Error image polarization areas are marked: 1,3,5 are under +10,+5,+1 V respectively and 2,4,6 are under -10,-5,-1 V respectively.

The scans of piezoresponse are shown in the table 4.3.9. In comparison to previous experiment, the response of this part of the sample was much smoother. Additionally, the footprints were not visible in out-of-plane phase channel. At the rest, the behavior of this part of the sample was the same as in previous experiment.

Table 4.3.9. AFM piezoresponse images of out-of-plane amplitude and phase (Amplitude1, Phase1), in-plane amplitude and phase (Amplitude2, Phase2) during polarization experiment; scan size 25 µm

	Out-of-plane amplitude	Out-of-plane phase	In-plane amplitude	In-plane phase
Before Polarization	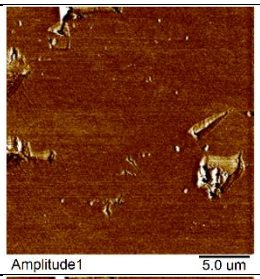	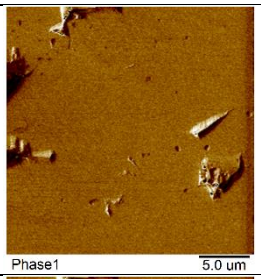	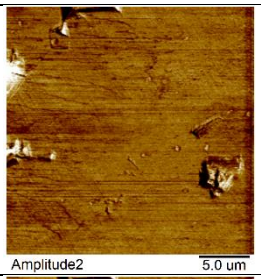	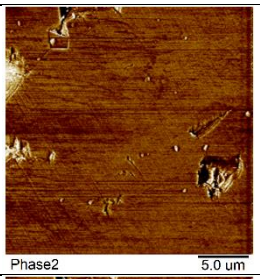
After Polarization on area1 (+10 V for 15 min)	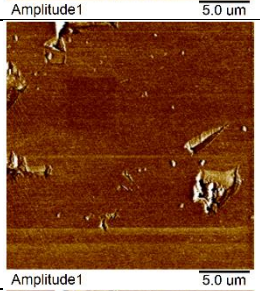	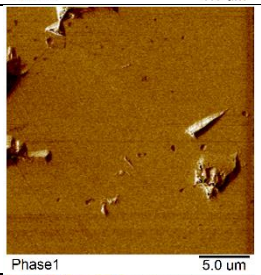	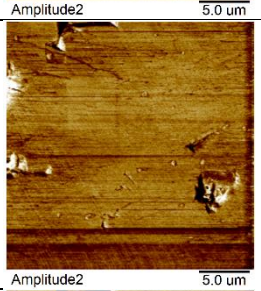	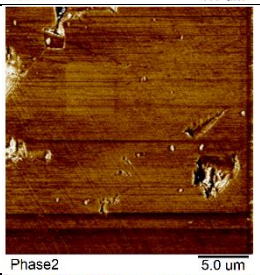
After Polarization on area2 (-10 V for 15 min)	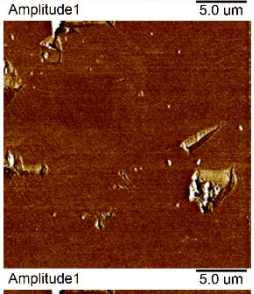	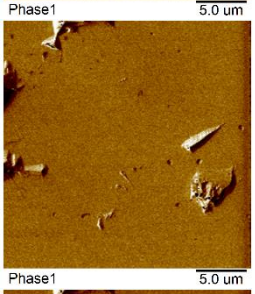	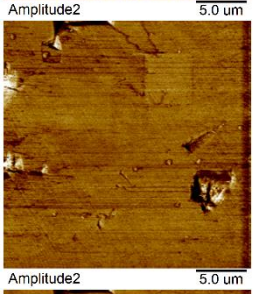	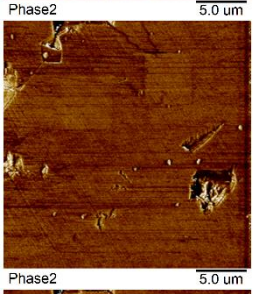
After Polarization on area3 (+5 V for 15 min)	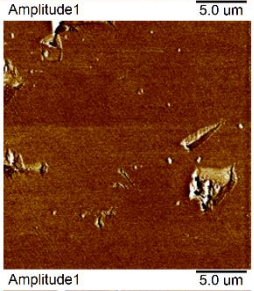	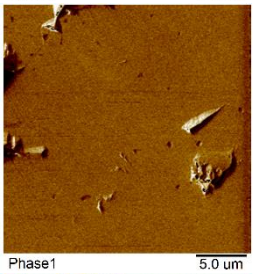	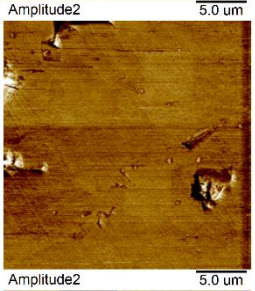	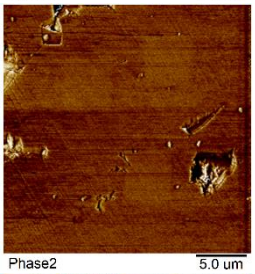
After Polarization on area4 (-5 V for 15 min)	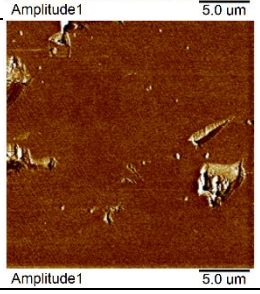	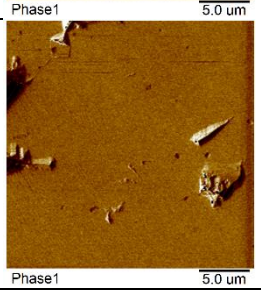	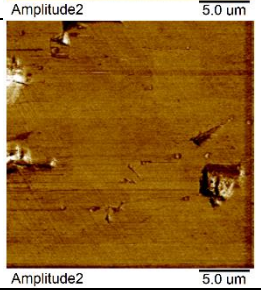	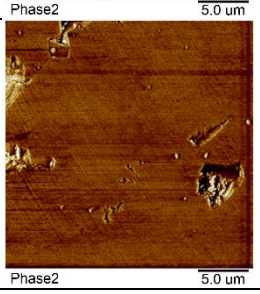

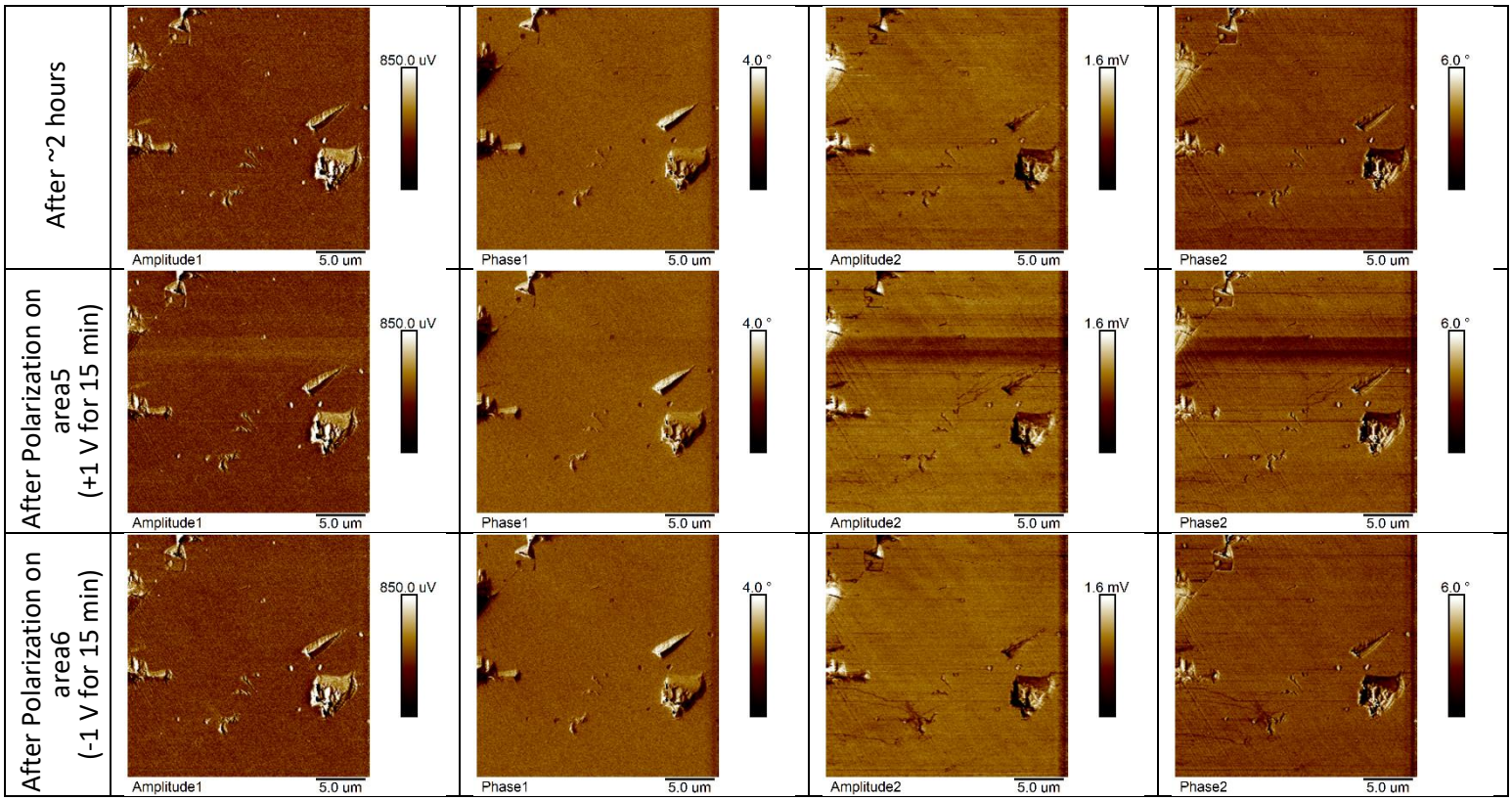

The piezoelectric response after applying electric field was weaker than the response of the same voltages in previous experiment. It took more time (~ 2 hours) for the footprint to be erased after applying ±5 V.

As the polarization after both positive and negative applied voltages is similar, we also consider that some electric charge was located at this part of the surface. The initial piezoresponse picture and polarization under additional electric field is hard to recognize. Also, footprints kept longer than in previous experiment, at which the measured area was farther to the electrode. Such piezoresponse behavior could depend on the distance between measured area and electric contact.

Finally, in PMN PT20 ceramic sample were found domains, which correspond to ferroelectric state. The rest part of the sample showed piezoelectric response similar to so called “clear area” of PZT single crystal. Nevertheless, both positive and negative additional electric field gave similar polarization footprint.

5 Conclusion

Ferroelectric samples of PZT single crystal and PMN PT20 ceramics were investigated by dielectric spectroscopy and PFM methods. During dielectric spectroscopy measurements the PMN PT20 ceramic showed high dielectric response stability over applied frequencies. The phase transition peak was seen in a wide range of temperatures (from 280 K to 360 K), which corresponds to the behavior of a relaxor. Moreover, additional electric field of 1 kV/cm was applied to the sample, which resulted in broadening of the peak of imaginary part of permittivity.

The single-crystal PZT 1.1 and ceramic PMN PT20 samples showed inhomogeneity on their surface during PFM measurements. Three areas with different piezoelectric response were found for PZT 1.1. They were called structural domains, changing spots and clear area. Each of them showed its own behavior during PFM measurements without additional electric field and also during polarization with external electric field.

Structural domains had specific shape and showed piezoresponse picture that did not change its shape with time or additional electric field. This picture was usually visible at frequencies lower than 50 kHz. The polarization experiment showed that applied electric field left piezoresponse footprint that was detected on scans of 25 µm size. Positive voltage left more recognizable footprint than negative. All of them disappeared after some time (~ 1 hour). The whole piezoresponse picture became harder to recognize during measurements.

So called “Changing spots” area showed the most unusual behavior. The piezoresponse picture was found at resonance frequency of the probe. The picture looked like spots of any shape and the shape was changing during measurements. The picture was depending on scanning direction but had some similarities for up and down measurements. Applying electric field did not create specific footprint but changed the whole piezoresponse picture, that also was changing its shape but more slowly than before.

So called “Clear area” did not show any specific piezoresponse picture: there was no stable domains or spots recognized on all piezoresponse channels at any of measured frequencies. Sometimes there appeared pictures that could suddenly disappear without

changing reasonable scanning parameters. Additional electric field left very weak footprint, that could be recognized in out-of-plane phase channel.

Two interesting areas were found, by PFM method at the surface of PMN PT20. One area showed domain spots that were seen on both in-plane and out-of-plane piezoresponse channels. The rest area was similar to the clear area of PZT 1.1. Without additional electric field it did not show any piezoresponse picture. The application of electric field at so called “clear area” created recognizable footprint that was better seen under positive than negative voltage. Moreover, both directions of applied electric field change the polarization of the sample surface in similar way.

The work has a lot of future perspectives for investigation of ferroelectric samples. It is recommended to improve piezoresponse scans quality by setting the equipment of AFM. Providing better connection between a sample and ground could reach higher contrast of piezoelectric images that may lead to some specific sample behavior (like disappearing figures) absence.

Moreover, the piezoresponse behavior of phase transition depending on temperature could be researched. This was never investigated on high temperatures by PFM method. It is required to connect heater and to achieve the temperatures of phase transition to investigate temperature evolution of domains. Furthermore, the measurements of switching ferroelectric domains of the samples by applying high density electric field could be provided. For this purpose an additional high voltage DC generator should be attached to the sample. All these experiments will provide better understanding of electric characteristics and physical mechanisms inside ferroelectric materials.

References

[1] A. A. Bokov and Z. G. Ye, “Recent progress in relaxor ferroelectrics with perovskite structure,” *J. Mater. Sci.*, vol. 41, no. 1, pp. 31–52, 2006, doi: 10.1007/s10853-005-5915-7.

[2] J. Briscoe and S. Dunn, “Piezoelectricity and Ferroelectricity,” Springer, Cham, 2014, pp. 3–17.

[3] J. Morra, “What is the Piezoelectric Effect? | Electronic Design,” *electronicdesign.com Manufaturing company Electronic design*. https://www.electronicdesign.com/power-management/article/21801833/what-is-the-piezoelectric-effect (accessed Mar. 02, 2021).

[4] S. Zhukov, “Piezoelectricity & Piezo Applications,” *americanpiezo.com, Manufaturing company APC International*. https://www.americanpiezo.com/knowledge-center/piezo-theory/piezoelectricity.html (accessed Mar. 02, 2021).

[5] J. Briscoe and S. Dunn, *Nanostructured Piezoelectric Energy Harvesters*. Cham: Springer International Publishing, 2014.

[6] K. Manchanda, “Ferroelectricity | physics,” *Encyclopedia Britannica*. https://www.britannica.com/science/ferroelectricity (accessed May 03, 2021).

[7] D. Damjanovic, “Ferroelectric, dielectric and piezoelectric properties of ferroelectric thin films and ceramics,” *Reports Prog. Phys.*, vol. 61, no. 11, pp. 1267–1324, 1998, doi: 10.1088/0034-4885/61/9/002.

[8] V. V. Xavier, “Piezoelectric and Ferroelectric Materials | Explorer Materials,” *explorermaterials.wordpress.com, Personal Web page*. https://explorermaterials.wordpress.com/basic-concepts/piezoelectric-and-ferroelectric-materials/ (accessed Apr. 30, 2021).

[9] B. Jaffe, R. S. Roth, and S. Marzullo, “Piezoelectric properties of Lead zirconate-Lead titanate solid-solution ceramics,” *Journal of Applied Physics*, vol. 25, no. 6. pp. 809–810, 1954, doi: 10.1063/1.1721741.

[10] O. E. Fesenko and V. G. Smotrakov, “Optic and dielectric study of lead zirconate crystals,” *Ferroelectrics*, vol. 12, no. 1, pp. 211–213, Jan. 1976, doi: 10.1080/00150197608241430.

[11] A. Manbachi and R. S. C. Cobbold, “Development and application of piezoelectric materials for ultrasound generation and detection,” *Ultrasound*, vol. 19, no. 4. pp. 187–196, Nov. 03, 2011, doi: 10.1258/ult.2011.011027.

[12] S. Wada *et al.*, “Phase transition behaviors of BaTiO3-BaZrO3 solid solutions under high direct current bias fields,” *J. Mater. Res.*, vol. 17, no. 2, pp. 456–464, 2002, doi: 10.1557/JMR.2002.0064.

[13] E. Sawaguchi, “Ferroelectricity versus Antiferroelectricity in the Solid Solutions of PbZrO3 and PbTi03,” *J. Phys. Soc. Japan*, vol. 8, no. 5, pp. 615–629, Dec. 1953, doi: 10.1143/JPSJ.8.615.

[14] C. Chung, *Microstructural Evolution in Lead Zirconate Titanate (PZT) Piezoelectric Ceramics*. University of Connecticut, 2014.

[15] S. Limpijumnong, S. Rujirawat, A. Boonchun, M. F. Smith, and B. Cherdhirunkorn, "Identification of Mn site in Pb (Zr,Ti)O3 by synchrotron x-ray absorption near-edge structure: Theory and experiment," *Appl. Phys. Lett.*, vol. 90, no. 10, 2007, doi: 10.1063/1.2711200.

[16] S. E. Park and T. R. Shrout, "Ultrahigh strain and piezoelectric behavior in relaxor based ferroelectric single crystals," *J. Appl. Phys.*, vol. 82, no. 4, pp. 1804–1811, Aug. 1997, doi: 10.1063/1.365983.

[17] Y. Namba and H. Takahashi, "Ultra-precision surface grinding of PMN-PT relaxor-based ferroelectric single crystals," *CIRP Ann. - Manuf. Technol.*, vol. 59, no. 1, pp. 589–592, Jan. 2010, doi: 10.1016/j.cirp.2010.03.143.

[18] H. Tan, H. Takenaka, C. Xu, W. Duan, I. Grinberg, and A. M. Rappe, "First-principles studies of the local structure and relaxor behavior of Pb(Mg1/3Nb2/3) O3-PbTiO3 - derived ferroelectric perovskite solid solutions," *Phys. Rev. B*, vol. 97, no. 17, May 2018, doi: 10.1103/PhysRevB.97.174101.

[19] S. B. Vakhrushev and R. G. Burkovskiy, "Structure and lattice dynamics of cubic ferroelectric relaxors," *Reports Prog. Phys.*, vol. 38, no. 10, p. 19, 2006.

[20] M. Algueró *et al.*, "Size effects on the macroscopic properties of the relaxor ferroelectric Pb(Mg1/3Nb2/3)O3-PbTiO3 solid solution," in *Handbook of Advanced Dielectric, Piezoelectric and Ferroelectric Materials: Synthesis, Properties and Applications*, Elsevier Ltd, 2008, pp. 447–471.

[21] A. Note, "Agilent Basics of Measuring the Dielectric Properties of Materials," *Agilent technologies*, p. 32, 2006.

[22] Y. Feldman, "Broad Band Dielectric Spectroscopy in Time and Frequency Domain," *Personal Web page*, 2016. https://yurifeldman.huji.ac.il/broad-band-dielectric-spectroscopy-time-and-frequency-domain (accessed May 04, 2021).

[23] M. A. Vasilyeva, I. V Lounev, and Y. A. Gusev, *The Methodology of the Experiment on the Dielectric Spectrometer Novocontrol BDS Concept 80 Part 1. Dielectric Measurements from 10-5 Hz to 3·10 9 Hz on the Dielectric spectrometer Novocontrol BDS Concept 80 Study guide*. Kazan: Kazan University, 2013.

[24] V. M. Radivojević, S. Rupčić, M. Srnović, and G. Benšić, "Measuring the dielectric constant of paper using a parallel plate capacitor," *Int. J. Electr. Comput. Eng. Syst.*, vol. 9, no. 1, pp. 1–10, 2018, doi: 10.32985/ijeces.9.1.1.

[25] Y. Feldman, "Lecture 7 i. The dielectric relaxation and dielectric resonance. ii. The distribution functions of the relaxation times. iii. Cole-Cole distribution.," *Personal Web page*, 2016. https://slideplayer.com/slide/4661464/ (accessed May 04, 2021).

[26] G. Binnig, C. F. Quate, and C. Gerber, "Atomic force microscope," *Phys. Rev. Lett.*, vol. 56, no. 9, pp. 930–933, Mar. 1986, doi: 10.1103/PhysRevLett.56.930.

[27] V. L. Mironov, *Basics of scanning probe microscopy*. Nizjniy Novgorod: Russian Science Academy, 2004.

[28] S. S. Horgan, “Atomic Force Microscopy,” *witec-instruments.com, Instrument company WITec*. https://www.witec.de/techniques/afm/ (accessed May 04, 2021).

[29] N. Jalili and K. Laxminarayana, “A review of atomic force microscopy imaging systems: Application to molecular metrology and biological sciences,” *Mechatronics*, vol. 14, no. 8, pp. 907–945, Oct. 2004, doi: 10.1016/j.mechatronics.2004.04.005.

[30] S. Magonov, “Piezoresponse Force Microscopy in Its Applications,” *ntmdt-si.com, Instrument company NT-MDT Development*, 2019. https://www.ntmdt-si.com/resources/applications/piezoresponse-force-microscopy-in-its-applications (accessed May 04, 2021).

[31] V. Grichko, “Piezoresponse force microscopy,” *Electronic Encyclopedia Wikiwand*, 2015. https://www.wikiwand.com/en/Piezoresponse_force_microscopy (accessed May 04, 2021).

[32] N. A. Pertsev *et al.*, “Dynamics of ferroelectric nanodomains in BaTiO 3 epitaxial thin films via piezoresponse force microscopy,” *IOP Publ. Ltd., Nanotechnol.*, vol. 19, no. 9, pp. 1–7, 2008, doi: 10.1088/0957-4484/19/37/375703.

[33] S. E. Park, “Piezoelectric Force Microscopy (PFM),” *parksystems.com, Instrument company Park Systems*, 2020. https://www.parksystems.com/park-spm-modes/93-dielectric-piezoelectric/230-piezoelectric-force-microscopy-pfm (accessed May 07, 2021).

[34] J. Perez de la Torre, P. Mantas, M. R. Soares, H. Amorin, M. E. . Costa, and A. M. R. Senos, “Growth of lead zirconate titanate single crystals by the high temperature solution method,” *Mater. Sci. Forum*, vol. 514, 2006.

[35] X. Liu *et al.*, “Aging behavior and mechanical properties of 0.69Pb(Mg1/3Nb 2/3)O3-0.31PbTiO3 ceramics,” *Ferroelectrics*, vol. 467, no. 1, pp. 115–125, 2014, doi: 10.1080/00150193.2014.932577.

[36] S. L. Swartz and T. R. Shrout, “Fabrication of perovskite lead magnesium niobate,” *Mater. Res. Bull.*, vol. 17, no. 10, pp. 1245–1250, Oct. 1982, doi: 10.1016/0025-5408(82)90159-3.